Journal of Computational Mathematics
Vol.44, No.1, 2026, 103–134.

http://www.global-sci.org/jcm
doi:10.4208/jcm.2410-m2024-0023

STABILIZATION-FREE VIRTUAL ELEMENT METHOD FOR THE TRANSMISSION EIGENVALUE PROBLEM ON ANISOTROPIC MEDIA*

Jian Meng[1)]
Department of Mathematics, College of Science, National University of Defense Technology, Changsha 410073, China
Email: mengjian23@nudt.edu.cn
Lei Guan
College of Computer Science and Technology, Taiyuan University of Technology, Taiyuan 030002, China
Email: guanleimath@163.com
Xu Qian and Songhe Song
Department of Mathematics, College of Science, National University of Defense Technology, Changsha 410073, China
Emails: qianxu@nudt.edu.cn, shsong@nudt.edu.cn
Liquan Mei
School of Mathematics and Statistics, Xi'an Jiaotong University, Xi'an 710049, China
Email: lqmei@mail.xjtu.edu.cn

Abstract

In this paper, we develop the stabilization-free virtual element method for the Helmholtz transmission eigenvalue problem on anisotropic media. The eigenvalue problem is a variable-coefficient, non-elliptic, non-selfadjoint and nonlinear model. Separating the cases of the index of refraction $n \neq 1$ and $n \equiv 1$, the stabilization-free virtual element schemes are proposed, respectively. Furthermore, we prove the spectral approximation property and error estimates in a unified theoretical framework. Finally, a series of numerical examples are provided to verify the theoretical results, show the benefits of the stabilization-free virtual element method applied to eigenvalue problems, and implement the extensions to high-order and high-dimensional cases.

Mathematics subject classification: 65N25, 65N30, 65N15.
Key words: Virtual element method, Stabilization-free, Transmission eigenvalue problem, Anisotropic media, Error estimates.

1. Introduction

The eigenvalue problems arising from partial differential equations (PDEs) play a fundamental role in engineering applications. The transmission eigenvalue problem (TEP) is essential in the conventional qualitative method of inverse scattering problems from the theoretical perspective, see monographs [23,30]. In particular, the changes about the constitutive parameters of the media lead to the corresponding changes in the measured transmission eigenvalues and hence transmission eigenvalues are useful for the nondestructive testing of inhomogeneous media. For the details how this procedure works, we refer to [23] again.

* Received January 31, 2024 / Revised version received June 15, 2024 / Accepted October 12, 2024 / Published online November 12, 2024 /
[1)] Corresponding author

The interest of this manuscript lies in the numerical analysis for the computation of the interior TEP on anisotropic media: Find non-trivial w, u and $k \in \mathbb{C} \setminus \{0\}$ such that

$$-\mathrm{div}(\boldsymbol{A}\nabla w) - k^2 n w = 0 \quad \text{in } \Omega, \tag{1.1a}$$

$$-\Delta u - k^2 u = 0 \quad \text{in } \Omega, \tag{1.1b}$$

$$w - u = 0 \quad \text{on } \partial\Omega, \tag{1.1c}$$

$$\frac{\partial w}{\partial \boldsymbol{\nu}_{\boldsymbol{A}}} - \frac{\partial u}{\partial \boldsymbol{\nu}} = 0 \quad \text{on } \partial\Omega. \tag{1.1d}$$

Here $\Omega \subseteq \mathbb{R}^d$ $(d = 2, 3)$ is a bounded simply connected domain with the boundary $\partial\Omega$. $\boldsymbol{A}$ is a $d \times d$ symmetric positive definite matrix with real $L^\infty(\Omega)$ entries. The index of refraction $n \in L^\infty(\Omega)$ is a positive real function, $\boldsymbol{\nu}$ is the unit outer normal to $\partial\Omega$ and $\partial w/\partial \boldsymbol{\nu}_{\boldsymbol{A}} = \boldsymbol{A}\nabla w \cdot \boldsymbol{\nu}$. The theoretical existence of transmission eigenvalues have been studied in [23, 24]. Moreover, the numerical computation is an interesting and nontrivial task since the problem possesses nonlinear, non-selfadjoint and non-elliptic properties.

Under the case of isotropic media, that is, $\boldsymbol{A}$ equals to the identity matrix $\boldsymbol{I}$, the first numerical study for the TEP refers to [31]. In recent years, various numerical methods have been applied to the TEP of isotropic media, for example, iterative method [51], finite element methods [43, 55, 57, 58] and spectral-element methods [3, 57]. Underlying the anisotropic scenario, it calls for individual numerical methods and approximation theory. A few numerical algorithms to compute transmission eigenvalues of anisotropic media have been proposed. In 2013, Ji and Sun [37] proposed a continuous finite element method and explicitly enforced the Dirichlet boundary condition to derive a large, sparse and non-Hermitian generalized matrix eigenvalue problem. Then they devised a more efficient multi-level approach to solve it. In 2017, Kleefeld and Colton [38] computed interior transmission eigenvalues for anisotropic media by using boundary integral equations and a nonlinear solver based on complex-valued contour integrals. They also considered the fundamental solutions method [39]. To date, there have been limited works in terms of the rigorous analysis of the convergence and the convergence rate of numerical schemes. Xie and Wu [56] defined the finite element approximation for the problem (1.1) and designed the multilevel correction method. Gong *et al.* [35] have formulated TEP of anisotropic media as a spectral problem of a holomorphic Fredholm operator and proved the convergence of the Lagrange linear finite element approximation by using the spectral approximation theory of holomorphic Fredholm operator, but without the optimal convergence rate. Furthermore, Meng and Mei [44] proposed the standard virtual element method to solve the TEP and applied the $\mathbb{T}$-coercivity theory to prove the a priori and a posteriori error estimates. Recently, Liu *et al.* [42] studied the convergence of the mixed finite element method for the TEP with the index of refraction $n \equiv 1$.

The virtual element method (VEM) is introduced in 2013 [8], which is the generalization of the finite element method to general polyhedral meshes. Except for the mere possibility to use polytopal meshes, the VEM is also attractive in some problems, for example, high-order PDEs, the construction of divergence-free requirement and complex geometric structures [12,25,28,40]. In the last ten years, the VEMs of elliptic problems [11], elasticity problems [26], fluidodynamics problems [12], magnetostatic problems [9] and coding aspects [10] have been widely investigated, also refer to recent monograph [4] for more details. The subject of the VEM approximation for eigenvalue problems is also an appealing field [4, Chapter 7]. To date, the VEM has been developed for different eigenvalue problems, for instance, the Steklov eigenvalue problem [40,47],

the Laplacian eigenvalue problem [34], the acoustic vibration problem [14], the vibration and buckling problems of Kirchhoff plate [49], the transmission eigenvalue problem on isotropic media [45, 48, 50] and the Stokes eigenvalue problem [41]. In particular, Meng and Mei [44] have proved the a priori and a posteriori error estimates for the Helmholtz TEP of anisotropic media under the following restrictions that (i) there exists a real number $\gamma > 1$ such that the matrix $\boldsymbol{A}$ and the index of refraction n satisfy $A_* > \gamma$ and $n_* > \gamma$ over Ω, (ii) there exists a real number $0 < \gamma < 1$ such that $\boldsymbol{A}$ and n satisfy $A^* < \gamma$ and $n^* < \gamma$ over Ω, where

$$A_* := \inf_{\boldsymbol{x}\in\Omega} \inf_{\boldsymbol{\xi}\in\mathbb{R}^d,|\boldsymbol{\xi}|=1} \big(\boldsymbol{\xi}\cdot\boldsymbol{A}(\boldsymbol{x})\boldsymbol{\xi}\big) > 0, \quad n_* := \inf_{\boldsymbol{x}\in\Omega} n(\boldsymbol{x}) > 0,$$
$$A^* := \sup_{\boldsymbol{x}\in\Omega} \sup_{\boldsymbol{\xi}\in\mathbb{R}^d,|\boldsymbol{\xi}|=1} \big(\boldsymbol{\xi}\cdot\boldsymbol{A}(\boldsymbol{x})\boldsymbol{\xi}\big) < \infty, \quad n^* := \sup_{\boldsymbol{x}\in\Omega} n(\boldsymbol{x}) < \infty,$$

which are quite restrictive. Meanwhile, leaving the case of the index of refraction $n \equiv 1$ opens for investigation. Note that this case is not a direct derivation of the existing works [44, 45, 48, 50]. One of the aims for the current paper is to close the gap.

The other aim of the manuscript is to investigate the stabilization-free VEM for the anisotropic TEP with both cases $n_* > \gamma > 1$ (or $n^* < \gamma < 1$) and $n \equiv 1$. As usual, a VEM bilinear form contains the consistency and stabilization terms, where the consistency on polynomial space is assured by the consistency term and the stability of the VEM scheme is guaranteed by the other depending on appropriate stability parameters. However, distinguishing from the associated source problems, there contain stabilization parameters on both sides of the VEM schemes for eigenvalue problems. As discussed in [14, 20, 34, 41, 46, 47], these stabilization parameters have dramatic effects on the VEM performance. To investigate good VEM approximation of eigenvalue problems, there require many observations and efforts about the suitable choices of stabilization parameters. For this reason, the goal of the present paper is to remove all stabilization terms in the VEM schemes of eigenvalue problems. Especially, more virtues of the stabilization-free VEM for the anisotropic TEP are demonstrated in numerical examples, see Section 5.3.

In this paper, we consider the stabilization-free VEM for the TEP on anisotropic media. Relying on the stabilization-free VEM [15,16], we devise the stabilization-free VEM scheme for the TEP. Therein, the enlarged enhancement VEM space is introduced by lifting the degree of the polynomial space containing the Laplacian of virtual functions and modified in a way as in [2] to admit the same dimension as the standard VEM space. By using a higher-order polynomial projection of the gradient of virtual functions, the stabilization-free VEM bilinear form is well defined, see Section 3.1, where the degree of the higher-order polynomial projection depends on the number of vertices of the used polygonal meshes. Further, the stabilization-free VEM schemes are given under two cases $n \neq 1$ and $n \equiv 1$, respectively. Moreover, the associated solution operators are proved to be well defined. By means of the discrete interpolant, the polynomial approximation, the discrete inf-sup condition and the spectral approximation theory, we derive the error estimates of eigenfunctions and eigenvalues. Our theoretical results are supported by a series of numerical tests, where shows the accuracy and robustness of the numerical method for different configurations, and the improvement of higher-order and higher-dimensional cases. Meanwhile, we also underline the advantages of the stabilization-free VEM to solve the TEP on anisotropic media.

This paper is organized as follows. In Section 2, we present the model problem. In Section 3, we introduce the stabilization-free VEM and investigate the well-defined property of discrete solution operators. In Section 4, we develop the error estimates of the numerical method. In

Section 5, we report numerical tests to verify our theoretical results. In Section 6, we finally highlight the conclusions of this research.

2. Model Problem and Weak Formulations

Throughout the paper, we employ the notation of the scalar Sobolev space $H^s(D)$ equipped with norm $\|\cdot\|_{s,D}$ and seminorm $|\cdot|_{s,D}$ in an open bounded domain D [21]. The space $H^0(D)$ coincides with the Lebesgue space $L^2(D)$. The inner product on $L^2(D)$ is denoted by $(\cdot,\cdot)_D$, and the inner product on the boundary ∂D is denoted by $\langle\cdot,\cdot\rangle_{\partial D}$. The subscripts D and ∂D will be omitted when D denotes the whole computational domain. As usual, we use bold fonts to express vector variables, operators and spaces. In what follows, for given two positive quantities a and b, we use the short-hand notation $a \lesssim b$ if there exists a positive constant C independent of the discretization parameters such that $a \le C\, b$.

In this section, the variational formulations for the TEP (1.1) are summarized briefly. Since the theoretical derivations are related to whether $n \neq 1$ or $n \equiv 1$, we separate the continuous problem into two cases as follows, respectively.

2.1. The case $n_* > \gamma > 1$ or $n^* < \gamma < 1$

Let us introduce the function space

$$\boldsymbol{V}_1 := \{(\psi, s) \in H^1(\Omega) \times H^1(\Omega) \,:\, \psi - s = 0 \text{ on } \partial\Omega\}$$

equipped with the norm

$$\|(\psi, s)\|_{\boldsymbol{V}_1} = \big(\|\psi\|_1^2 + \|s\|_1^2\big)^{\frac{1}{2}}.$$

For any $(\psi, s) \in \boldsymbol{V}_1$, we test (1.1a) and (1.1b) by $\psi \in H^1(\Omega)$ and $s \in H^1(\Omega)$, respectively, to arrive at

$$(\boldsymbol{A}\nabla w, \nabla\psi) + (nw, \psi) - \left\langle \frac{\partial w}{\partial \boldsymbol{\nu}_{\mathbf{A}}}, \psi \right\rangle = \lambda(nw, \psi), \tag{2.1}$$

$$(\nabla u, \nabla s) + (u, s) - \left\langle \frac{\partial u}{\partial \boldsymbol{\nu}}, s \right\rangle = \lambda(u, s), \tag{2.2}$$

where denoting $\lambda := k^2 + 1$. Then the boundary condition (1.1d) derives the variational form of (1.1) as follows: Find non-zero $(w, u) \in \boldsymbol{V}_1$ and $\lambda \in \mathbb{C}$ such that

$$\mathbb{A}_1\big((w, u), (\psi, s)\big) = \lambda \mathbb{B}_1\big((w, u), (\psi, s)\big), \quad \forall\, (\psi, s) \in \boldsymbol{V}_1, \tag{2.3}$$

where two bilinear forms are denoted by

$$\begin{aligned}
\mathbb{A}_1\big((w, u), (\psi, s)\big) &:= (\boldsymbol{A}\nabla w, \nabla\psi) + (nw, \psi) - (\nabla u, \nabla s) - (u, s),\\
\mathbb{B}_1\big((w, u), (\psi, s)\big) &:= (nw, \psi) - (u, s).
\end{aligned}$$

For the sake of theoretical analysis, we now concentrate on the case (i) that there exists a real number $\gamma > 1$ such that the matrix $\boldsymbol{A}$ and the index of refraction n satisfy $A_* > \gamma$ and $n_* > \gamma$ over Ω. For the other case (ii), all the following mathematical derivations can be presented in the same way, since these two cases seem to be structurally similar.

Furthermore, the associated continuous solution operator $\boldsymbol{T}_1 : \boldsymbol{V}_1 \to \boldsymbol{V}_1$ can be defined by

$$\mathbb{A}_1\big(\boldsymbol{T}_1(\varphi, r), (\psi, s)\big) = \mathbb{B}_1\big((\varphi, r), (\psi, s)\big), \quad \forall\, (\psi, s) \in \boldsymbol{V}_1. \tag{2.4}$$

Next we discuss that this solution operator $\boldsymbol{T}_1$ is well defined. Because $\mathbb{A}_1((\cdot\,,\cdot),(\cdot\,,\cdot))$ is not coercive over $\boldsymbol{V}_1$, we introduce a bounded operator $\mathbb{T}(\psi,s) := (\psi, 2\psi - s)$ on $\boldsymbol{V}_1$. Therefore, the existence and uniqueness of solution for the associate source problem are guaranteed by the theory of the $\mathbb{T}$-coercivity [29, Section 2.2].

Proposition 2.1. *Let $\boldsymbol{A} \in \boldsymbol{W}^{1,\infty}(\Omega)$, then for any given $(\varphi, r) \in \boldsymbol{V}_1$, the associate source problem* (2.4) *has a unique solution $(\varphi^s, r^s) \in \boldsymbol{V}_1$, that is, $\boldsymbol{T}_1(\varphi, r) = (\varphi^s, r^s)$ satisfying*

$$\|(\varphi^s, r^s)\|_{\boldsymbol{V}_1} \lesssim \|\varphi\|_{-1} + \|r\|_{-1}. \tag{2.5}$$

Furthermore, suppose that $\boldsymbol{A} = a\boldsymbol{I}$ ($a \neq 1$ is a constant), there holds true

$$\|\varphi^s\|_{1+\theta} + \|r^s\|_{1+\theta} \lesssim \|(\varphi, r)\|_{\boldsymbol{V}_1}, \tag{2.6}$$

where θ is a constant dependent of the domain shape, and shall be fixed in the proof.

Proof. By lending the definition of $\mathbb{T}$, the condition $A_*, n_* > \gamma > 1$ and the Young's inequality with $\varepsilon \in (1/\gamma, 1)$, basic derivations give

$$\begin{aligned}
\mathbb{A}_1\big((\psi,s),\mathbb{T}(\psi,s)\big) &= (\boldsymbol{A}\nabla\psi,\nabla\psi) + (n\psi,\psi) - \big(\nabla s,\nabla(2\psi - s)\big) - (s, 2\psi - s)\\
&\geq \gamma\|\psi\|_1^2 + \|s\|_1^2 - 2(\nabla s,\nabla\psi) - 2(s,\psi)\\
&\geq \left(\gamma - \frac{1}{\varepsilon}\right)\|\psi\|_1^2 + (1-\varepsilon)\|s\|_1^2 \gtrsim \|(\psi,s)\|_{\boldsymbol{V}_1}^2.
\end{aligned} \tag{2.7}$$

With the $\mathbb{T}$-coercivity at hand, the assertion of the existence and uniqueness follows from the classical theory of the $\mathbb{T}$-coercivity [29, Theorem 1] arriving at

$$\|(\varphi^s, r^s)\|_{\boldsymbol{V}_1} \lesssim \|\varphi\|_{-1} + \|r\|_{-1}. \tag{2.8}$$

On the other hand, the difference $w - u$ satisfies

$$\Delta(w-u) = k^2 u - \frac{k^2 n}{a} w \quad \text{in } \Omega, \tag{2.9a}$$

$$w - u = 0 \qquad\qquad\qquad\quad \text{on } \partial\Omega, \tag{2.9b}$$

which associates to the source problem with homogeneous Dirichlet boundary values and satisfying $\Delta(\varphi^s - r^s) = k^2 r - (k^2 n/a)\varphi$. Then there exists a constant $r_\Omega > 0$ such that $\varphi^s - r^s \in H^{1+\theta}(\Omega)$ with $\theta \in (0, r_\Omega)$ and

$$\|\varphi^s - r^s\|_{1+\theta} \lesssim \|(\varphi, r)\|_{\boldsymbol{V}_1}, \tag{2.10}$$

where $r_\Omega \geq 1$ when the domain Ω is convex, while it is at least $\pi/\omega - \varepsilon$ (for any $\varepsilon > 0$) for the non-convex domain with maximum interior angle $\omega < 2\pi$. Actually, this theory comes from the regularity estimate of the second-order elliptic problem (see [1, Chapter 9]). Besides, the term $aw - u$ satisfies

$$\Delta(aw-u) = k^2 u - k^2 n w \quad \text{in } \Omega, \tag{2.11a}$$

$$\frac{\partial(aw-u)}{\partial\boldsymbol{\nu}} = 0 \qquad\qquad\quad \text{on } \partial\Omega, \tag{2.11b}$$

which associates to the source problem with homogeneous Neumann boundary values and satisfying $\Delta(a\varphi^s - r^s) = k^2 r - k^2 n\varphi$. Based on the version of the above regularity result [53, Proposition 7.7] for the Neumann boundary condition, we conclude the mapping $(k^2 r - k^2 n\varphi) \mapsto (a\varphi^s - r^s)$ is also bounded from $L^2(\Omega)$ into $H^{1+\theta}(\Omega)$. Since $a \neq 1$, then the mapping $(\varphi, r) \mapsto (\varphi^s, r^s)$ is bounded from $L^2(\Omega) \times L^2(\Omega)$ into $H^{1+\theta}(\Omega) \times H^{1+\theta}(\Omega)$, that is,

$$\|\varphi^s\|_{1+\theta} + \|r^s\|_{1+\theta} \lesssim \|(\varphi, r)\|_{\boldsymbol{V}_1}. \tag{2.12}$$

Thus, we complete the proof. □

Remark 2.1. If $A^*, n^* < \gamma < 1$, there provides a hint to construct the bounded operator $\mathbb{T}(\psi, s) := (\psi - 2s, -s)$, then the same techniques can be applied to close the proof.

2.2. The case $n \equiv 1$

In this case, the inequality (2.7) is not correct any more, which leads that the well-defined property of the corresponding solution operator does not hold true. Dating back to 2009, Cakoni *et al.* [22] considered basic theory for (1.1) with $n \equiv 1$ by providing an appropriate substitution. Let $\boldsymbol{u} := \boldsymbol{A}\nabla w - \nabla u$ and $\lambda := k^2$, then the eigenvalue problem (1.1) can be restated as a fourth-order problem: Find $\boldsymbol{u}$ and λ such that

$$(\nabla \mathrm{div}\cdot + \lambda \boldsymbol{A}^{-1})(\boldsymbol{A}^{-1} - \boldsymbol{I})^{-1}(\nabla \mathrm{div}\cdot + \lambda)\boldsymbol{u} = 0 \quad \text{in } \Omega, \tag{2.13a}$$

$$\mathrm{div}\,\boldsymbol{u} = 0, \quad \boldsymbol{u}\cdot\boldsymbol{\nu} = 0 \qquad \text{on } \partial\Omega. \tag{2.13b}$$

Recalling that if $A^* < \gamma < 1$ or $A_* > \gamma > 1$, the problem (2.13) admits an infinite countable set of real transmission eigenvalues with $+\infty$ as the only one accumulation point [22]. We here focus on the case of $A^* < \gamma < 1$. As for $A_* > \gamma > 1$, it is also essentially resemble and does not hide other difficulties, see [42, Section 2.2]. Following [42], we introduce the auxiliary variables

$$\varphi := \mathrm{div}\,\boldsymbol{u}, \quad \boldsymbol{y} := \lambda\boldsymbol{u},$$
$$\boldsymbol{p} := (\boldsymbol{A}^{-1} - \boldsymbol{I})^{-1}\nabla\varphi + \big(\boldsymbol{I} + (\boldsymbol{A}^{-1} - \boldsymbol{I})^{-1}\big)\boldsymbol{y}.$$

Let $r \in H^1(\Omega) \cap L^2_0(\Omega)$ satisfy the orthogonal decomposition $\boldsymbol{p} = \nabla r + (\nabla r)^\perp$ with $(\nabla r)^\perp \in [\nabla(H^1(\Omega) \cap L^2_0(\Omega))]^\perp$. For brevity, we denote the matrix $(\boldsymbol{A}^{-1} - \boldsymbol{I})^{-1}$ as $\boldsymbol{P}$ in the following. Then the variational form is rewritten as: Find

$$(\lambda, \varphi, \boldsymbol{y}, r) \in \mathbb{C} \times \big[H^1_0(\Omega) \cap L^2_0(\Omega)\big] \times \boldsymbol{L}^2(\Omega) \times \big[H^1(\Omega) \cap L^2_0(\Omega)\big]$$

such that

$$(\boldsymbol{P}\nabla\varphi, \nabla\psi) + (\boldsymbol{P}\boldsymbol{y}, \nabla\psi) = \lambda\big((\varphi, \psi) + (r, \psi)\big), \quad \forall\, \psi \in H^1_0(\Omega) \cap L^2_0(\Omega), \tag{2.14a}$$

$$(\boldsymbol{P}\nabla\varphi, \boldsymbol{z}) + \big((\boldsymbol{I} + \boldsymbol{P})\boldsymbol{y}, \boldsymbol{z}\big) - (\nabla r, \boldsymbol{z}) = 0, \qquad \forall\, \boldsymbol{z} \in \boldsymbol{L}^2(\Omega), \tag{2.14b}$$

$$-(\boldsymbol{y}, \nabla s) = \lambda(\varphi, s), \qquad \forall\, s \in H^1(\Omega) \cap L^2_0(\Omega). \tag{2.14c}$$

Next we write (2.14) as a more compact form: Find $(\lambda, \varphi, \boldsymbol{y}, r) \in \mathbb{C} \times \boldsymbol{V}_2$ such that

$$\mathbb{A}_2\big((\varphi, \boldsymbol{y}, r), (\psi, \boldsymbol{z}, s)\big) = \lambda\mathbb{B}_2\big((\varphi, \boldsymbol{y}, r), (\psi, \boldsymbol{z}, s)\big), \quad \forall\, (\psi, \boldsymbol{z}, s) \in \boldsymbol{V}_2, \tag{2.15}$$

where $\boldsymbol{V}_2 := [H_0^1(\Omega) \cap L_0^2(\Omega)] \times \boldsymbol{L}^2(\Omega) \times [H^1(\Omega) \cap L_0^2(\Omega)]$ and

$$\begin{aligned}\mathbb{A}_2\big((\varphi, \boldsymbol{y}, r), (\psi, \boldsymbol{z}, s)\big) &:= (\boldsymbol{P}\nabla\varphi, \nabla\psi) + (\boldsymbol{P}\boldsymbol{y}, \nabla\psi) + (\boldsymbol{P}\nabla\varphi, \boldsymbol{z}) \\ &\quad + \big((\boldsymbol{I}+\boldsymbol{P})\boldsymbol{y}, \boldsymbol{z}\big) - (\nabla r, \boldsymbol{z}) - (\boldsymbol{y}, \nabla s), \\ \mathbb{B}_2\big((\varphi, \boldsymbol{y}, r), (\psi, \boldsymbol{z}, s)\big) &:= (\varphi, \psi) + (r, \psi) + (\varphi, s).\end{aligned}$$

For any $(\psi, \boldsymbol{z}, s) \in \boldsymbol{V}_2$, we introduce the norm $\|\cdot\|_{\boldsymbol{V}_2}$ denoted by

$$\|(\psi, \boldsymbol{z}, s)\|_{\boldsymbol{V}_2} = \big(\|\psi\|_1^2 + \|\boldsymbol{z}\|_0^2 + \|s\|_1^2\big)^{\frac{1}{2}}.$$

To prove error estimates of the non-selfadjoint problem, we consider the adjoint problem of (2.15): Find $(\lambda^*, \varphi^*, \boldsymbol{y}^*, r^*) \in \mathbb{C} \times \boldsymbol{V}_2$ such that

$$\mathbb{A}_2\big((\psi, \boldsymbol{z}, s), (\varphi^*, \boldsymbol{y}^*, r^*)\big) = \overline{\lambda^*}\mathbb{B}_2\big((\psi, \boldsymbol{z}, s), (\varphi^*, \boldsymbol{y}^*, r^*)\big), \quad \forall\, (\psi, \boldsymbol{z}, s) \in \boldsymbol{V}_2, \tag{2.16}$$

where $\overline{\lambda^*}$ denotes the complex conjugate of λ^*. Then we introduce an other continuous solution operator $\boldsymbol{T}_2 : \boldsymbol{V}_2 \to \boldsymbol{V}_2$ defined by

$$\mathbb{A}_2\big(\boldsymbol{T}_2(\varphi, \boldsymbol{y}, r), (\psi, \boldsymbol{z}, s)\big) = \mathbb{B}_2\big((\varphi, \boldsymbol{y}, r), (\psi, \boldsymbol{z}, s)\big), \quad \forall\, (\psi, \boldsymbol{z}, s) \in \boldsymbol{V}_2. \tag{2.17}$$

Proposition 2.2. *Let $\boldsymbol{P} \in \boldsymbol{W}^{2,\infty}(\Omega)$, then for any given $(\varphi, \boldsymbol{y}, r) \in \boldsymbol{V}_2$, the associate source problem* (2.17) *has a unique solution $(\varphi^s, \boldsymbol{y}^s, r^s) \in \boldsymbol{V}_2$, that is, $\boldsymbol{T}_2(\varphi, \boldsymbol{y}, r) = (\varphi^s, \boldsymbol{y}^s, r^s)$, satisfying*

$$\|(\varphi^s, \boldsymbol{y}^s, r^s)\|_{\boldsymbol{V}_2} \lesssim \|\varphi\|_{-1} + \|r\|_{-1}. \tag{2.18}$$

Furthermore, suppose that $\boldsymbol{A} = a\boldsymbol{I}$ ($a \neq 1$ is a constant), there holds true

$$\|\varphi^s\|_{1+\theta} + \|\boldsymbol{y}^s\|_\theta + \|r^s\|_{1+\theta} \lesssim \|(\varphi, \boldsymbol{y}, r)\|_{\boldsymbol{V}_2}, \tag{2.19}$$

where $\theta \in (0, 1)$ shall be introduced in the proof.

Proof. By splitting the bilinear form $\mathbb{A}_2((\cdot,\cdot,\cdot),(\cdot,\cdot,\cdot))$ as the sum of the following three parts:

$$\mathbb{A}_2\big((\varphi, \boldsymbol{y}, r), (\psi, \boldsymbol{z}, s)\big) = a\big((\varphi, \boldsymbol{y}), (\psi, \boldsymbol{z})\big) + b\big((\psi, \boldsymbol{z}), r\big) + b\big((\varphi, \boldsymbol{y}), s\big), \tag{2.20}$$

where

$$\begin{aligned}a\big((\varphi, \boldsymbol{y}), (\psi, \boldsymbol{z})\big) &= (\boldsymbol{P}\nabla\varphi, \nabla\psi) + (\boldsymbol{P}\boldsymbol{y}, \nabla\psi) + (\boldsymbol{P}\nabla\varphi, \boldsymbol{z}) + \big((\boldsymbol{I}+\boldsymbol{P})\boldsymbol{y}, \boldsymbol{z}\big), \\ b\big((\varphi, \boldsymbol{y}), s\big) &= -(\boldsymbol{y}, \nabla s).\end{aligned}$$

Then the following Brezzi-Babuška conditions hold true:

$$\big|a\big((\varphi, \boldsymbol{y}), (\psi, \boldsymbol{z})\big)\big| \lesssim \|(\varphi, \boldsymbol{y})\|_{H^1(\Omega)\times L^2(\Omega)}\|(\psi, \boldsymbol{z})\|_{H^1(\Omega)\times L^2(\Omega)}, \tag{2.21}$$

$$\big|b\big((\varphi, \boldsymbol{y}), s\big)\big| \lesssim \|(\varphi, \boldsymbol{y})\|_{H^1(\Omega)\times L^2(\Omega)}\|s\|_1, \tag{2.22}$$

$$\big|a\big((\varphi, \boldsymbol{y}), (\varphi, \boldsymbol{y})\big)\big| \gtrsim \|(\varphi, \boldsymbol{y})\|^2_{H^1(\Omega)\times L^2(\Omega)}, \tag{2.23}$$

$$\sup_{(\varphi,\boldsymbol{y})\in[H_0^1(\Omega)\cap L_0^2(\Omega)]\times\boldsymbol{L}^2(\Omega)} \frac{b\big((\varphi, \boldsymbol{y}), s\big)}{\|(\varphi, \boldsymbol{y})\|_{H^1(\Omega)\times L^2(\Omega)}} \gtrsim \|s\|_1. \tag{2.24}$$

It immediately follows by the Brezzi-Babuška theory [18, Part Three] or [19, Section 4.2] that (2.17) admits a unique solution $(\varphi^s, \boldsymbol{y}^s, r^s) \in \boldsymbol{V}_2$ satisfying (2.18).

Next we show in details the proof of (2.19) that is fundamental for the spectral approximation. For any smooth enough function $\boldsymbol{v}$, basic computation gives

$$\boldsymbol{\Delta}\boldsymbol{v} = \nabla \mathrm{div}\, \boldsymbol{v} - \mathrm{curl}(\mathrm{rot}\, \boldsymbol{v}).$$

In view of $\boldsymbol{u} = \boldsymbol{A}\nabla w - \nabla u$, we have $\mathrm{rot}\, \boldsymbol{u} = 0$, which implies that $\boldsymbol{\Delta}\boldsymbol{u} = \nabla \mathrm{div}\, \boldsymbol{u}$. With this in hand, we simplify (2.13a) and then state (2.13) in the variational form as follows: Find $\lambda \in \mathbb{C}$ and $\boldsymbol{u} \in \mathcal{H}_0(\Omega)$ such that

$$\int_\Omega \boldsymbol{P}(\boldsymbol{\Delta} + \lambda)\boldsymbol{u} \cdot (\boldsymbol{\Delta} + \lambda \boldsymbol{A}^{-1})\boldsymbol{v}\, \mathrm{d}\Omega = 0, \quad \forall\, \boldsymbol{v} \in \mathcal{H}_0(\Omega), \tag{2.25}$$

where

$$\mathcal{H}_0(\Omega) := \big\{\boldsymbol{v} \in \boldsymbol{H}(\mathrm{div}, \Omega) \,:\, \mathrm{div}\, \boldsymbol{v} \in H_0^1(\Omega),\ \boldsymbol{v} \cdot \boldsymbol{\nu} = 0 \text{ on } \partial\Omega\big\}.$$

Using the denseness in $\mathcal{H}_0(\Omega)$ of C^∞ functions with compact support on Ω, we can obtain the equivalence between (2.13) and (2.25), i.e. $\boldsymbol{u} \in \mathcal{H}_0(\Omega)$ satisfies (2.25) for each $\boldsymbol{v} \in \mathcal{H}_0(\Omega)$ if and only if $\boldsymbol{u}$ satisfies the fourth-order problem (2.13). Equivalently, we can write (2.25) as

$$\mathcal{B}_\lambda(\boldsymbol{u}, \boldsymbol{v}) = \lambda \mathcal{C}_\lambda(\boldsymbol{u}, \boldsymbol{v}), \quad \forall\, \boldsymbol{v} \in \mathcal{H}_0(\Omega), \tag{2.26}$$

where

$$\mathcal{B}_\lambda(\boldsymbol{u}, \boldsymbol{v}) = \int_\Omega \boldsymbol{P}(\boldsymbol{\Delta} + \lambda)\boldsymbol{u} \cdot (\boldsymbol{\Delta} + \lambda)\boldsymbol{v}\, \mathrm{d}\Omega + \lambda^2 \int_\Omega \boldsymbol{u}\boldsymbol{v}\, \mathrm{d}\Omega, \tag{2.27}$$

$$\mathcal{C}_\lambda(\boldsymbol{u}, \boldsymbol{v}) = \int_\Omega \mathrm{div}\, \boldsymbol{u}\, \mathrm{div}\, \boldsymbol{v}\, \mathrm{d}\Omega. \tag{2.28}$$

Under the assumptions on $\boldsymbol{P}$, there exists a constant $\alpha > 0$ such that

$$\begin{aligned}\mathcal{B}_\lambda(\boldsymbol{u}, \boldsymbol{u}) &\gtrsim \alpha\|(\boldsymbol{\Delta} + \lambda)\boldsymbol{u}\|_0^2 + \|\boldsymbol{u}\|_0^2 \geq \alpha\|\boldsymbol{\Delta}\boldsymbol{u}\|_0^2 - 2\alpha\|\boldsymbol{\Delta}\boldsymbol{u}\|_0\|\boldsymbol{u}\|_0 + (\alpha+1)\|\boldsymbol{u}\|_0^2 \\ &= \epsilon\left(\|\boldsymbol{u}\|_0 - \frac{\alpha}{\epsilon}\|\boldsymbol{\Delta}\boldsymbol{u}\|_0\right)^2 + \left(\alpha - \frac{\alpha^2}{\epsilon}\right)\|\boldsymbol{\Delta}\boldsymbol{u}\|_0^2 + (1 + \alpha - \epsilon)\|\boldsymbol{u}\|_0^2,\end{aligned}$$

where ϵ belongs to $(\alpha, \alpha+1)$. Setting $\epsilon = \alpha + 1/2$, we arrive at

$$\lambda\|\mathrm{div}, \boldsymbol{u}\|_0^2 \overset{(2.26)}{=} \mathcal{B}_\lambda(\boldsymbol{u}, \boldsymbol{u}) \gtrsim \frac{\alpha}{1+2\alpha}\big(\|\boldsymbol{\Delta}\boldsymbol{u}\|_0^2 + \|\boldsymbol{u}\|_0^2\big). \tag{2.29}$$

Recalling that $\varphi = \mathrm{div}\, \boldsymbol{u}$, (2.29) implies that

$$\|\boldsymbol{\Delta}\boldsymbol{u}\|_0 + \|\boldsymbol{u}\|_0 \lesssim \|\varphi\|_0. \tag{2.30}$$

Let us introduce the interpolation space $[\boldsymbol{H}^1(\Omega), \boldsymbol{L}^2(\Omega)]_\theta$ between $\boldsymbol{H}^1(\Omega)$ and $\boldsymbol{L}^2(\Omega)$ (see [19, Remark 4.3.15]) with the norm

$$\|\boldsymbol{p}\|_{[\boldsymbol{H}^1(\Omega), \boldsymbol{L}^2(\Omega)]_\theta} = \sup_{a>0} \inf_{\boldsymbol{p}_1 \in \boldsymbol{H}^1(\Omega)} \big(a^{-\theta}\|\boldsymbol{p} - \boldsymbol{p}_1\|_0 + a^{1-\theta}\|\boldsymbol{p}_1\|_1\big),$$

then it is clear that $\boldsymbol{H}^\theta(\Omega) \hookrightarrow [\boldsymbol{H}^1(\Omega), \boldsymbol{L}^2(\Omega)]_\theta$. By applying (2.30) and the fact $\mathrm{div}\, \boldsymbol{u} \in H_0^1(\Omega)$ satisfying the Poincaré inequality $\|\mathrm{div}\, \boldsymbol{u}\|_0 \lesssim \|\nabla\, \boldsymbol{u}\|_0$, we have

$$\begin{aligned}\|\nabla\varphi\|_{[\boldsymbol{H}^1(\Omega), \boldsymbol{L}^2(\Omega)]_\theta} &= \sup_{a>0} \inf_{\boldsymbol{p}_1 \in \boldsymbol{H}^1(\Omega)} \big(a^{-\theta}\|\nabla\varphi - \boldsymbol{p}_1\|_0 + a^{1-\theta}\|\boldsymbol{p}_1\|_1\big) \\ &\lesssim \sup_{a>0} \big(a^{-\theta}(\|\boldsymbol{\Delta}\boldsymbol{u}\|_0 + \|\mathrm{div}\, \boldsymbol{u}\|_0) + a^{1-\theta}\|\mathrm{div}\, \boldsymbol{u}\|_1\big) \\ &\lesssim \sup_{a>0}(a^{-\theta} + a^{1-\theta})\|\varphi\|_0,\end{aligned} \tag{2.31}$$

where we observe $\|\nabla\varphi\|_{[\boldsymbol{H}^1(\Omega),\boldsymbol{L}^2(\Omega)]_\theta}$ can be bounded in terms of the constant a, that is, the desired priori estimate holds true

$$\|\varphi\|_{1+\theta} \lesssim \|(\varphi,\boldsymbol{y},r)\|_{\boldsymbol{V}_2}. \tag{2.32}$$

Since $C_0^\infty(\Omega)\times\boldsymbol{L}^2(\Omega)\times C_0^\infty(\Omega)$ is dense in $\boldsymbol{V}_2$, then for any $(\varphi,\boldsymbol{y},r)\in\boldsymbol{V}_2$, there is $(\varphi_j,\boldsymbol{y},r_j)\in C_0^\infty(\Omega)\times\boldsymbol{L}^2(\Omega)\times C_0^\infty(\Omega)$ such that

$$\|(\varphi_j,\boldsymbol{y},r_j)-(\varphi,\boldsymbol{y},r)\|_{\boldsymbol{V}_2} \;\to\; 0 \quad\text{as}\quad j\;\to\;\infty. \tag{2.33}$$

Let $\boldsymbol{u}_j^s$ be the solution when $(\varphi_j,\boldsymbol{y},r_j)$ is associated to the right-hand term of the related source problem of (2.26). By introducing the similar auxiliary variables $\varphi_j^s=\operatorname{div}\boldsymbol{u}_j^s$, $\boldsymbol{y}_j^s=\lambda\boldsymbol{u}_j^s$, and $\boldsymbol{p}_j^s=\boldsymbol{P}\nabla\varphi_j^s+(\boldsymbol{I}+\boldsymbol{P})\boldsymbol{y}_j^s$, it follows by the same procedures to derive

$$\begin{aligned}
&\big(\boldsymbol{P}\nabla\varphi_j^s,\nabla\psi\big)+\big(\boldsymbol{P}\boldsymbol{y}_j^s,\nabla\psi\big)=(\varphi_j,\psi)+(r_j,\psi), && \forall\,\psi\in H_0^1(\Omega)\cap L_0^2(\Omega), && \text{(2.34a)}\\
&\big(\boldsymbol{P}\nabla\varphi_j^s,\boldsymbol{z}\big)+\big((\boldsymbol{I}+\boldsymbol{P})\boldsymbol{y}_j^s,\boldsymbol{z}\big)-\big(\nabla r_j^s,\boldsymbol{z}\big)=0, && \forall\,\boldsymbol{z}\in\boldsymbol{L}^2(\Omega), && \text{(2.34b)}\\
&-\big(\boldsymbol{y}_j^s,\nabla s\big)=(\varphi_j,s), && \forall\,s\in H^1(\Omega)\cap L_0^2(\Omega), && \text{(2.34c)}
\end{aligned}$$

where $r_j^s\in C_0^\infty(\Omega)\cap H^1(\Omega)\cap L_0^2(\Omega)$ still satisfies the orthogonal decomposition $\boldsymbol{p}_j^s=\nabla r_j^s+(\nabla r_j^s)^\perp$. According to (2.32) and (2.33), there exist $\varphi^s\in H^{1+\theta}(\Omega)\cap H_0^1(\Omega)\cap L_0^2(\Omega)$ and $r^s\in H^{1+\theta}(\Omega)\cap H^1(\Omega)\cap L_0^2(\Omega)$ such that

$$\begin{aligned}
&\big\|\varphi_j^s-\varphi^s\big\|_{1+\theta} \;\to\; 0, \quad \big\|r_j^s-r^s\big\|_{1+\theta} \;\to\; 0 \quad\text{as}\quad j\;\to\;\infty,\\
&\text{with}\quad \|\varphi^s\|_{1+\theta}+\|\boldsymbol{y}^s\|_\theta+\|r^s\|_{1+\theta}\lesssim\|(\varphi,\boldsymbol{y},r)\|_{\boldsymbol{V}_2}.
\end{aligned}$$

Thus, we complete the proof. □

As a direct consequence, the solution operator $\boldsymbol{T}_2$ is well defined and compact over $\boldsymbol{V}_2$ (see also [42, Lemma 2.1]).

3. Stabilization-free Virtual Element Approximation

Let $\mathcal{T}_h$ be a decomposition of the computational region Ω into nonoverlapping polygons with standard mesh regularity assumptions [2,8]. For each element $E\in\mathcal{T}_h$, its measure and diameter are denoted by $|E|$ and h_E, respectively. Meanwhile, the set ∂E represents the collection of all boundary edges of E and V_i $(i=1,\ldots,N_E^V)$ denotes the i-th vertex of E. For a geometric object D (for instance, an 1-dimensional edge or a 2-dimensional element), $\mathbb{P}_\ell(D)$ denotes the space of all polynomials of the degree less than or equal to $\ell\in\mathbb{N}$.

3.1. Stabilization-free virtual element space and bilinear forms

This subsection is devoted to introducing the stabilization-free VEM based to the ideas in [15,16,26,27]. We begin with defining a projection operator $\Pi_{\ell,E}^\nabla: H^1(E)\to\mathbb{P}_\ell(E)$ satisfying, for any $v\in H^1(E)$, for any $p_\ell\in\mathbb{P}_\ell(E)$,

$$\int_E\nabla\big(\Pi_{\ell,E}^\nabla v-v\big)\cdot\nabla p_\ell\mathrm{d}E=0, \quad P_0\big(\Pi_{\ell,E}^\nabla v-v\big)=0, \tag{3.1}$$

where $P_0(v)=\int_{\partial E}v|_{\partial E}\mathrm{d}s/|\partial E|$ for $\ell=1$, meanwhile $P_0(v)=(v,1)_E/|E|$ for $\ell\geq 2$.

For any element $E \in \mathcal{T}_h$, we define the enlarged enhancement virtual element space by

$$V_h(E) = \Big\{ v_h \in H^1(E) \cap C^0(\partial E) \,:\, v_h|_e \in \mathbb{P}_1(e),\ \forall\, e \in \partial E,\ \Delta v_h \in \mathbb{P}_{1+l}(E), \\ \int_E \big(v_h - \Pi^{\nabla}_{1,E} v_h\big) p_{1+l}\,\mathrm{d}E = 0,\ \forall\, p_{1+l} \in \mathbb{P}_{1+l}(E) \Big\}, \quad (3.2)$$

where $l \in \mathbb{N}$ is a given parameter depending on the total number N_E^V of all vertices of the element E. The associated degrees of freedom are assigned as the values of v_h at all vertices of the polygonal element E [2, 16, 26, 27]. With the local space, we construct the global stabilization-free virtual element space as

$$V_h = \big\{ v_h \in H^1(\Omega) : v_h|_E \in V_h(E),\ \forall\, E \in \mathcal{T}_h \big\}. \quad (3.3)$$

To define the VEM scheme, we introduce vector and scalar polynomial projections $\boldsymbol{\Pi}^0_{\ell,E} : [L^2(E)]^2 \to [\mathbb{P}_\ell(E)]^2$ and $\Pi^0_{\ell,E} : L^2(E) \to \mathbb{P}_\ell(E)$ defined by

$$\int_E \big(\boldsymbol{\Pi}^0_{\ell,E}\boldsymbol{v} - \boldsymbol{v}\big)\boldsymbol{p}_\ell\,\mathrm{d}E = 0, \quad \forall\, \boldsymbol{v} \in [L^2(E)]^2, \quad \forall\, \boldsymbol{p}_\ell \in [\mathbb{P}_\ell(E)]^2, \quad (3.4)$$

$$\int_E \big(\Pi^0_{\ell,E} v - v\big) p_\ell\,\mathrm{d}E = 0, \quad \forall\, v \in L^2(E), \quad \forall\, p_\ell \in \mathbb{P}_\ell(E), \quad (3.5)$$

respectively. In a similar way, the $\boldsymbol{L}^2$-polynomial projection $\boldsymbol{\Pi}^0_{l,E}$ of degree l is denoted by

$$\int_E \big(\boldsymbol{\Pi}^0_{l,E}\boldsymbol{v} - \boldsymbol{v}\big)\boldsymbol{p}_l\,\mathrm{d}E = 0, \quad \forall\, \boldsymbol{v} \in [L^2(E)]^2, \quad \forall\, \boldsymbol{p}_l \in [\mathbb{P}_l(E)]^2. \quad (3.6)$$

The following results reside from the theory developed in [16, 26, 27].

Proposition 3.1. *Assume that the following condition:*

$$2l + 2 \geq N_E^V - 1 \quad (3.7)$$

holds true for any element $E \in \mathcal{T}_h$, then the stability inequality is valid

$$\|\nabla v_h\|_{0,E} \lesssim \big\|\boldsymbol{\Pi}^0_{l,E}\nabla v_h\big\|_{0,E} \lesssim \|\nabla v_h\|_{0,E}, \quad \forall\, v_h \in V_h(E). \quad (3.8)$$

For any matrix $\boldsymbol{M} \in \mathbb{R}^{2\times 2}$, any elements $u_h, v_h \in V_h(E)$ and $\boldsymbol{y}_h \in [\mathbb{P}_l(E)]^2$, the following discrete bilinear forms on the element level are introduced by:

$$a_h^{\boldsymbol{M},E}(u_h, v_h) = \big(\boldsymbol{M}\boldsymbol{\Pi}^0_{l,E}\nabla u_h, \boldsymbol{\Pi}^0_{l,E}\nabla v_h\big)_E,$$
$$b_h^{\boldsymbol{M},E}(\boldsymbol{y}_h, u_h) = \big(\boldsymbol{M}\boldsymbol{y}_h, \boldsymbol{\Pi}^0_{l,E}\nabla u_h\big)_E,$$
$$c_h^E(u_h, v_h) = \big(\Pi^0_{1,E}u_h, \Pi^0_{1,E}v_h\big)_E.$$

The globally discrete bilinear forms $a_h^{\boldsymbol{M}}(\cdot\,,\cdot), b_h^{\boldsymbol{M}}(\cdot\,,\cdot)$ and $c_h(\cdot\,,\cdot)$ can be defined by summing the local contributions of $a_h^{\boldsymbol{M},E}(\cdot\,,\cdot), b_h^{\boldsymbol{M},E}(\cdot\,,\cdot)$ and $c_h^E(\cdot\,,\cdot)$, respectively. If $\boldsymbol{M}$ equals to the identity matrix $\boldsymbol{I}$, the mathematical symbol $\boldsymbol{M}$ will be removed. As usual, the global polynomial projections can be locally defined by restricting onto every element, for example, $\boldsymbol{\Pi}^0_l|_E := \boldsymbol{\Pi}^0_{l,E}$.

Based on the above statement, we investigate the stabilization-free VEM for the TEP on anisotropic media.

3.2. The case $n_* > \gamma > 1$ or $n^* < \gamma < 1$

In view of the stabilization-free virtual element space V_h, we introduce the vector discrete space as

$$\boldsymbol{V}_1^h = \{(u_h, v_h) \in V_h \times V_h \,:\, (u_h - v_h)|_e = 0,\ \forall\, e \in \partial\Omega\}.$$

Further, the stabilization-free VEM scheme of the model problem (2.3) is to find non-zero $(w_h, u_h) \in \boldsymbol{V}_1^h$ and $\lambda_h \in \mathbb{C}$ such that

$$\mathbb{A}_1^h\big((w_h, u_h), (\psi_h, s_h)\big) = \lambda_h \mathbb{B}_1^h\big((w_h, u_h), (\psi_h, s_h)\big), \quad \forall\, (\psi_h, s_h) \in \boldsymbol{V}_1^h, \tag{3.9}$$

where

$$\begin{aligned}
&\mathbb{A}_1^h\big((w_h, u_h), (\psi_h, s_h)\big) := a_h^{\boldsymbol{A}}(w_h, \psi_h) + c_h(nw_h, \psi_h) - a_h(u_h, s_h) - c_h(u_h, s_h),\\
&\mathbb{B}_1^h\big((w, u), (\psi, s)\big) := c_h(nw_h, \psi_h) - c_h(u_h, s_h).
\end{aligned}$$

Next we study the $\mathbb{T}$-coercivity of the VEM bilinear form $\mathbb{A}_1^h((\cdot\,,\cdot), (\cdot\,,\cdot))$. The stability condition (3.8) and the Cauchy-Schwartz inequality ensure that

$$\begin{aligned}
&\big|\mathbb{A}_1^h\big((\psi_h, s_h), \mathbb{T}(\psi_h, s_h)\big)\big|\\
&\gtrsim \gamma\|\psi_h\|_1^2 + \|s_h\|_1^2 - 2(\|\nabla\psi_h\|_0\|\nabla s_h\|_0 + \|\psi_h\|_0\|s_h\|_0)\\
&\geq \gamma\|\psi\|_1^2 + \|s_h\|_1^2 - \left(\frac{1}{\varepsilon}\|\psi_h\|_1^2 + \varepsilon\|s_h\|_1^2\right)\\
&= \left(\gamma - \frac{1}{\varepsilon}\right)\|\psi_h\|_1^2 + (1-\varepsilon)\|s_h\|_1^2 \gtrsim \|(\psi_h, s_h)\|_{\boldsymbol{V}_1}^2,
\end{aligned}$$

where the parameter ε corresponds to the Young's inequality. By means of $\mathbb{T}$-coercivity theory [29, Theorem 2], the discrete inf-sup condition is valid

$$\sup_{(\psi_h,\varphi_h)\in\boldsymbol{V}_1^h} \frac{\big|\mathbb{A}_1^h\big((w_h, u_h), (\psi_h, \varphi_h)\big)\big|}{\|(\psi_h, \varphi_h)\|_{\boldsymbol{V}_1}} \gtrsim \|(w_h, u_h)\|_{\boldsymbol{V}_1}, \quad \forall\, (w_h, u_h) \in \boldsymbol{V}_1^h, \tag{3.10}$$

and then the associated discrete solution operator $\boldsymbol{T}_1^h : \boldsymbol{V}_1 \to \boldsymbol{V}_1^h \subseteq \boldsymbol{V}_1$ is well defined: For any given $(\varphi, r) \in \boldsymbol{V}_1$, there is

$$\mathbb{A}_1^h\big(\boldsymbol{T}_1^h(\varphi, r), (\psi_h, s_h)\big) = \mathbb{B}_1^h\big((\varphi, r), (\psi_h, s_h)\big), \quad \forall\, (\psi_h, s_h) \in \boldsymbol{V}_1^h. \tag{3.11}$$

3.3. The case $n \equiv 1$

Concerning the eigenvalue problem (2.14), the VEM scheme is to seek $(\lambda_h, \varphi_h, \boldsymbol{y}_h, r_h) \in \mathbb{C} \times \hat{V}_{h,0} \times [\mathbb{P}_l(\Omega)]^2 \times \hat{V}_h$ such that

$$a_h^{\boldsymbol{P}}(\varphi_h, \psi_h) + b_h^{\boldsymbol{P}}(\boldsymbol{y}_h, \psi_h) = \lambda_h\big(c_h(\varphi_h, \psi_h) + c_h(r_h, \psi_h)\big), \quad \forall\, \psi_h \in \hat{V}_{h,0}, \tag{3.12a}$$

$$b_h^{\boldsymbol{P}}(\boldsymbol{z}_h, \varphi_h) + \big((\boldsymbol{I} + \boldsymbol{P})\boldsymbol{y}_h, \boldsymbol{z}_h\big) - b_h(\boldsymbol{z}_h, r_h) = 0, \quad \forall\, \boldsymbol{z}_h \in [\mathbb{P}_l(\Omega)]^2, \tag{3.12b}$$

$$-b_h(\boldsymbol{y}_h, s_h) = \lambda_h c_h(\varphi_h, s_h), \quad \forall\, s_h \in \hat{V}_h, \tag{3.12c}$$

where the discrete spaces are defined by $\hat{V}_{h,0} := V_h \cap H_0^1(\Omega) \cap L_0^2(\Omega)$ and $\hat{V}_h := V_h \cap L_0^2(\Omega)$. Also, the VEM scheme can be rewritten as the following compact formulation: Find $(\lambda_h, \varphi_h, \boldsymbol{y}_h, r_h) \in \mathbb{C} \times \boldsymbol{V}_2^h$ such that for any $(\psi_h, \boldsymbol{z}_h, s_h) \in \boldsymbol{V}_2^h$,

$$\mathbb{A}_2^h\big((\varphi_h, \boldsymbol{y}_h, r_h), (\psi_h, \boldsymbol{z}_h, s_h)\big) = \lambda_h \mathbb{B}_2^h\big((\varphi_h, \boldsymbol{y}_h, r_h), (\psi_h, \boldsymbol{z}_h, s_h)\big), \tag{3.13}$$

where $\boldsymbol{V}_2^h := \hat{V}_{h,0} \times [\mathbb{P}_l(\Omega)]^2 \times \hat{V}_h$ and

$$\begin{aligned}\mathbb{A}_2^h\big((\varphi_h, \boldsymbol{y}_h, r_h), (\psi_h, \boldsymbol{z}_h, s_h)\big) &:= a_h^{\boldsymbol{P}}(\varphi_h, \psi_h) + b_h^{\boldsymbol{P}}(\boldsymbol{y}_h, \psi_h) + b_h^{\boldsymbol{P}}(\boldsymbol{z}_h, \varphi_h) \\ &\quad + \big((\boldsymbol{I}+\boldsymbol{P})\boldsymbol{y}_h, \boldsymbol{z}_h\big) - b_h(\boldsymbol{z}_h, r_h) - b_h(\boldsymbol{y}_h, s_h), \\ \mathbb{B}_2^h\big((\varphi_h, \boldsymbol{y}_h, r_h), (\psi_h, \boldsymbol{z}_h, s_h)\big) &:= c_h(\varphi_h, \psi_h) + c_h(r_h, \psi_h) + c_h(\varphi_h, s_h).\end{aligned}$$

The adjoint problem of (3.13) is to find $(\lambda_h^*, \varphi_h^*, \boldsymbol{y}_h^*, r_h^*) \in \mathbb{C} \times \boldsymbol{V}_2^h$ such that for any $(\psi_h, \boldsymbol{z}_h, s_h) \in \boldsymbol{V}_2^h$,

$$\mathbb{A}_2^h\big((\psi_h, \boldsymbol{z}_h, s_h), (\varphi_h^*, \boldsymbol{y}_h^*, r_h^*)\big) = \overline{\lambda_h^*}\, \mathbb{B}_2^h\big((\psi_h, \boldsymbol{z}_h, s_h), (\varphi_h^*, \boldsymbol{y}_h^*, r_h^*)\big). \tag{3.14}$$

Furthermore, for any $(\psi_h, \boldsymbol{z}_h, s_h) \in \boldsymbol{V}_2^h$, the discrete solution operator $\boldsymbol{T}_2^h : \boldsymbol{V}_2 \to \boldsymbol{V}_2^h \subseteq \boldsymbol{V}_2$ is defined by

$$\mathbb{A}_2^h\big(\boldsymbol{T}_2^h(\varphi, \boldsymbol{y}, r), (\psi_h, \boldsymbol{z}_h, s_h)\big) = \mathbb{B}_2^h\big((\varphi, \boldsymbol{y}, r), (\psi_h, \boldsymbol{z}_h, s_h)\big). \tag{3.15}$$

We need to discuss that the discrete solution operator is well defined. Indeed, basic computation derives

$$\begin{aligned}&a_h^{\boldsymbol{P},E}(\varphi_h, \varphi_h) + b_h^{\boldsymbol{P},E}(\boldsymbol{y}_h, \varphi_h) + b_h^{\boldsymbol{P},E}(\boldsymbol{y}_h, \varphi_h) + \big((\boldsymbol{I}+\boldsymbol{P})\boldsymbol{y}_h, \boldsymbol{y}_h\big)_E \\ &= \big\|(\boldsymbol{P} + A^*\boldsymbol{I})^{-\frac{1}{2}}\boldsymbol{P}\boldsymbol{\Pi}_{l,E}^0\nabla\varphi_h + (\boldsymbol{P} + A^*\boldsymbol{I})^{\frac{1}{2}}\boldsymbol{y}_h\big\|_{0,E}^2 + (1 - A^*)\|\boldsymbol{y}_h\|_{0,E}^2 \\ &\quad + \big(\big(\boldsymbol{P} - \boldsymbol{P}(\boldsymbol{P} + A^*\boldsymbol{I})^{-1}\boldsymbol{P}\big)\boldsymbol{\Pi}_{l,E}^0\nabla\varphi_h, \boldsymbol{\Pi}_{l,E}^0\nabla\varphi_h\big)_E \\ &\gtrsim \big\|\boldsymbol{\Pi}_{l,E}^0\nabla\varphi_h\big\|_{0,E}^2 + \|\boldsymbol{y}_h\|_{0,E}^2 \overset{(3.8)}{\gtrsim} \|\varphi_h\|_{1,E}^2 + \|\boldsymbol{y}_h\|_{0,E}^2.\end{aligned} \tag{3.16}$$

Besides, given $s_h \in \hat{V}_h$, apply $\boldsymbol{y}_h = -\boldsymbol{\Pi}_{l,E}^0\nabla s_h$ and the Poincaré inequality to obtain

$$-\big(\boldsymbol{y}_h, \boldsymbol{\Pi}_{l,E}^0\nabla s_h\big)_E = \|\boldsymbol{y}_h\|_{0,E}\big\|\boldsymbol{\Pi}_{l,E}^0\nabla s_h\big\|_{0,E} \overset{(3.8)}{\gtrsim} \|\boldsymbol{y}_h\|_{0,E}\|s_h\|_{1,E},$$

which implies that

$$\sup_{(\varphi_h, \boldsymbol{y}_h) \in \hat{V}_{h,0} \times [\mathbb{P}_l(\Omega)]^2} \frac{-\big(\boldsymbol{y}_h, \boldsymbol{\Pi}_l^0\nabla s_h\big)}{\|\varphi_h\|_1 + \|\boldsymbol{y}_h\|_0} \gtrsim \sup_{(\varphi_h, \boldsymbol{y}_h) \in \hat{V}_{h,0} \times [\mathbb{P}_l(\Omega)]^2} \frac{\|s_h\|_1\|\boldsymbol{y}_h\|_0}{\|\varphi_h\|_1 + \|\boldsymbol{y}_h\|_0} \gtrsim \|s_h\|_1. \tag{3.17}$$

Similarly, we have following inf-sup condition:

$$\sup_{(\psi_h, \boldsymbol{z}_h) \in \hat{V}_{h,0} \times [\mathbb{P}_l(\Omega)]^2} \frac{-\big(\boldsymbol{\Pi}_l^0\nabla r_h, \boldsymbol{z}_h\big)}{\|\psi_h\|_1 + \|\boldsymbol{z}_h\|_0} \gtrsim \|r_h\|_1. \tag{3.18}$$

Based on (3.16)-(3.18), we conclude the discrete inf-sup condition: For any $(\varphi_h, \boldsymbol{y}_h, r_h) \in \boldsymbol{V}_2^h$,

$$\sup_{(\psi_h, \boldsymbol{z}_h, s_h) \in \boldsymbol{V}_2^h} \frac{\big|\mathbb{A}_2^h\big((\varphi_h, \boldsymbol{y}_h, r_h), (\psi_h, \boldsymbol{z}_h, s_h)\big)\big|}{\|(\psi_h, \boldsymbol{z}_h, s_h)\|_{\boldsymbol{V}_2}} \gtrsim \|(\varphi_h, \boldsymbol{y}_h, r_h)\|_{\boldsymbol{V}_2}. \tag{3.19}$$

As a consequence, the discrete solution operator $\boldsymbol{T}_2^h$ related to the eigenvalue problem (3.13) is well defined.

4. Error Estimates

In this section, we shall prove the spectral approximation for the stabilization-free VEM. To this purpose, we present the following useful results.

Recalling the polynomial approximation error [21, 47] under the standard mesh regularity: For $v \in H^{1+\epsilon}(E)$ with $0 \le \epsilon \le \ell$, there exists $v_\pi \in \mathbb{P}_\ell(E)$ such that

$$\|v - v_\pi\|_{0,E} + h_E|v - v_\pi|_{1,E} \lesssim h_E^{1+\epsilon}\|v\|_{1+\epsilon,E}. \tag{4.1}$$

The interpolation estimate for the local stabilization-free virtual element space $V_h(E)$ is presented in the literature [16, Lemma 7] without proof. For the sake of completeness, we provide the error estimate for the interpolation to the stabilization-free virtual element space. Let v_c be the standard nodal interpolant to the Lagrange linear finite element space based on the auxiliary triangulation of the element E, and the error estimate of v_c is well known (see [21]) as follows:

$$\|v - v_c\|_{0,E} + h_E|v - v_c|_{1,E} \lesssim h_E^{1+\epsilon}\|v\|_{1+\epsilon,E}, \quad 0 \le \epsilon \le 1. \tag{4.2}$$

We consider function $v_I \in V_h(E)$ defined by the local problem

$$\begin{cases} \Delta v_I = \Delta \Pi^0_{3+l,E} v & \text{in } E, \\ v_I = v_c & \text{on } \partial E. \end{cases} \tag{4.3}$$

Then we present a brief proof of the interpolation estimate.

Proposition 4.1. *For $v \in H^{1+\epsilon}(E), 0 \le \epsilon \le 1$, there is $v_I \in V_h(E)$ such that*

$$\|v - v_I\|_{0,E} + h_E|v - v_I|_{1,E} \lesssim h_E^{1+\epsilon}\|v\|_{1+\epsilon,E}. \tag{4.4}$$

Proof. By (4.3) and integrating by parts, we have

$$\big(\nabla(v_I - v_c), \nabla(v_I - v_c)\big)_E = \big(\nabla\big(\Pi^0_{3+l,E} v - v_c\big), \nabla(v_I - v_c)\big)_E,$$

which implies that $|v_I - v_c|_{1,E} \le |\Pi^0_{3+l,E} v - v_c|_{1,E}$. With this in hand, there holds

$$\begin{aligned} |v - v_I|_{1,E} &\le |v - v_c|_{1,E} + |v_c - v_I|_{1,E} \\ &\le |v - v_c|_{1,E} + \big|\Pi^0_{3+l,E} v - v_c\big|_{1,E} \\ &\le 2|v - v_c|_{1,E} + \big|\Pi^0_{3+l,E} v - v\big|_{1,E} \overset{(4.1),(4.2)}{\lesssim} h_E^{\epsilon}\|v\|_{1+\epsilon,E}. \end{aligned}$$

Immediately, the desired estimate (4.4) is a simple consequence of the Poincaré-type argument. The proof is complete. □

Next, we are going to prove the error estimates of the stabilization-free VEM. Since we can apply the same framework of theoretical analysis for these two cases $n \ne 1$ and $n \equiv 1$, we only present the arguments for $n \equiv 1$, i.e. the continuous eigenvalue problem (2.15) and the associated stabilization-free VEM scheme (3.13). Noticing that the theoretical analysis in the present work calls for the obtained results in Propositions 2.1 and 2.2, where we considered the restricted condition $\boldsymbol{A} = a\boldsymbol{I}$ ($a \ne 1$ is a constant), therefore we still assume the above conditions to complete the theoretical proof. However, the assumptions in numerical examples are weaker than the theoretical requires.

It is common to split the convergence analysis for eigenvalue problems into two steps. On the first step, we consider the error bound for the corresponding source problems between (2.17) and (3.15) to study the convergence of the stabilization-free VEM. For any given $(\varphi, \boldsymbol{y}, r) \in \boldsymbol{V}_2$, we denote

$$(\varphi^s, \boldsymbol{y}^s, r^s) := \boldsymbol{T}_2(\varphi, \boldsymbol{y}, r), \quad \big(\varphi_h^s, \boldsymbol{y}_h^s, r_h^s\big) := \boldsymbol{T}_2^h(\varphi, \boldsymbol{y}, r). \tag{4.5}$$

The following theorem proves the error estimates.

Theorem 4.1. *Assume that*

$$(\varphi^s, \boldsymbol{y}^s, r^s),\ \big(\varphi_h^s, \boldsymbol{y}_h^s, r_h^s\big) \in \boldsymbol{V}_2 \cap \big(H^{1+\theta}(\Omega) \times [H^{\theta}(\Omega)]^2 \times H^{1+\theta}(\Omega)\big), \quad \theta > 0,$$

the following bound holds true:

$$\big\|\big(\varphi^s - \varphi_h^s, \boldsymbol{y}^s - \boldsymbol{y}_h^s, r^s - r_h^s\big)\big\|_{\boldsymbol{V}_2} \lesssim h^{\min\{\theta,1\}} \|(\varphi, \boldsymbol{y}, r)\|_{\boldsymbol{V}_2}. \tag{4.6}$$

Proof. Let $(\tilde{\varphi}_h^s, \tilde{\boldsymbol{y}}_h^s, \tilde{r}_h^s), (\psi_h, \boldsymbol{z}_h, s_h)$ be arbitrary elements in $\boldsymbol{V}_2^h$ and $(\sigma_h, \boldsymbol{\tau}_h, \varrho_h) \in \boldsymbol{V}_2^h$ satisfy

$$\begin{aligned}
&\mathbb{A}_2^h\big((\sigma_h, \boldsymbol{\tau}_h, \varrho_h), (\psi_h, \boldsymbol{z}_h, s_h)\big) \\
&= \mathbb{A}_2\big((\varphi^s, \boldsymbol{y}^s, r^s), (\psi_h, \boldsymbol{z}_h, s_h)\big) - \mathbb{A}_2^h\big((\tilde{\varphi}_h^s, \tilde{\boldsymbol{y}}_h^s, \tilde{r}_h^s), (\psi_h, \boldsymbol{z}_h, s_h)\big) \\
&\quad + \mathbb{B}_2^h\big((\varphi, \boldsymbol{y}, r), (\psi_h, \boldsymbol{z}_h, s_h)\big) - \mathbb{B}_2\big((\varphi, \boldsymbol{y}, r), (\psi_h, \boldsymbol{z}_h, s_h)\big).
\end{aligned} \tag{4.7}$$

By the discrete inf-sup inequality (3.19) and employing (4.7), we have

$$\begin{aligned}
\|(\sigma_h, \boldsymbol{\tau}_h, \varrho_h)\|_{\boldsymbol{V}_2} &\lesssim \sup_{(\psi_h, \boldsymbol{z}_h, s_h) \in \boldsymbol{V}_2^h} \frac{\big|\mathbb{A}_2^h\big((\sigma_h, \boldsymbol{\tau}_h, \varrho_h), (\psi_h, \boldsymbol{z}_h, s_h)\big)\big|}{\|(\psi_h, \boldsymbol{z}_h, s_h)\|_{\boldsymbol{V}_2}} \qquad (4.8)\\
&\lesssim \sup_{(\psi_h, \boldsymbol{z}_h, s_h) \in \boldsymbol{V}_2^h} \Bigg(\frac{\big|\mathbb{A}_2^h\big((\tilde{\varphi}_h^s, \tilde{\boldsymbol{y}}_h^s, \tilde{r}_h^s), (\psi_h, \boldsymbol{z}_h, s_h)\big) - \mathbb{A}_2\big((\varphi^s, \boldsymbol{y}^s, r^s), (\psi_h, \boldsymbol{z}_h, s_h)\big)\big|}{\|(\psi_h, \boldsymbol{z}_h, s_h)\|_{\boldsymbol{V}_2}} \\
&\qquad + \frac{\big|\mathbb{B}_2^h\big((\varphi, \boldsymbol{y}, r), (\psi_h, \boldsymbol{z}_h, s_h)\big) - \mathbb{B}_2\big((\varphi, \boldsymbol{y}, r), (\psi_h, \boldsymbol{z}_h, s_h)\big)\big|}{\|(\psi_h, \boldsymbol{z}_h, s_h)\|_{\boldsymbol{V}_2}} \Bigg).
\end{aligned}$$

It follows from (2.17) and (4.7) that

$$\mathbb{A}_2^h\big(\big(\sigma_h + \tilde{\varphi}_h^s, \boldsymbol{\tau}_h + \tilde{\boldsymbol{y}}_h^s, \varrho_h + \tilde{r}_h^s\big), (\psi_h, \boldsymbol{z}_h, s_h)\big) = \mathbb{B}_2^h\big((\varphi, \boldsymbol{y}, r), (\psi_h, \boldsymbol{z}_h, s_h)\big). \tag{4.9}$$

Therefore, we obtain $(\varphi_h^s, \boldsymbol{y}_h^s, r_h^s) = (\sigma_h + \tilde{\varphi}_h^s, \boldsymbol{\tau}_h + \tilde{\boldsymbol{y}}_h^s, \varrho_h + \tilde{r}_h^s)$ by the uniqueness of the solution to the source problem (3.15). By taking $(\tilde{\varphi}_h^s, \tilde{\boldsymbol{y}}_h^s, \tilde{r}_h^s) = ((\varphi^s)_I, (\boldsymbol{y}^s)_\pi, (r^s)_I) \in \boldsymbol{V}_2^h$, which satisfy the approximation results (4.1) and (4.4), we infer

$$\begin{aligned}
&\big\|\big(\varphi^s - \tilde{\varphi}_h^s, \boldsymbol{y}^s - \tilde{\boldsymbol{y}}_h^s, r^s - \tilde{r}_h^s\big)\big\|_{\boldsymbol{V}_2} \\
&= \big(\big\|\varphi^s - (\varphi^s)_I\big\|_1^2 + \big\|\boldsymbol{y}^s - (\boldsymbol{y}^s)_\pi\big\|_0^2 + \big\|r^s - (r^s)_I\big\|_1^2\big)^{\frac{1}{2}} \\
&\lesssim h^{\min\{\theta,1\}}\big(\|\varphi^s\|_{1+\theta} + \|\boldsymbol{y}^s\|_\theta + \|r^s\|_{1+\theta}\big) \overset{(2.19)}{\lesssim} h^{\min\{\theta,1\}} \|(\varphi, \boldsymbol{y}, r)\|_{\boldsymbol{V}_2}.
\end{aligned} \tag{4.10}$$

Moreover, we compute

$$\begin{aligned}
&\|(\sigma_h, \boldsymbol{\tau}_h, \varrho_h)\|_{\boldsymbol{V}_2} \\
&\overset{(4.8)}{\lesssim} \sup_{(\psi_h, \boldsymbol{z}_h, s_h) \in \boldsymbol{V}_2^h} \Bigg(\frac{\big|\mathbb{A}_2^h\big(\big((\varphi^s)_I, (\boldsymbol{y}^s)_\pi, (r^s)_I\big), (\psi_h, \boldsymbol{z}_h, s_h)\big) - \mathbb{A}_2\big((\varphi^s, \boldsymbol{y}^s, r^s), (\psi_h, \boldsymbol{z}_h, s_h)\big)\big|}{\|(\psi_h, \boldsymbol{z}_h, s_h)\|_{\boldsymbol{V}_2}} \\
&\qquad + \frac{\big|\mathbb{B}_2^h\big((\varphi, \boldsymbol{y}, r), (\psi_h, \boldsymbol{z}_h, s_h)\big) - \mathbb{B}_2\big((\varphi, \boldsymbol{y}, r), (\psi_h, \boldsymbol{z}_h, s_h)\big)\big|}{\|(\psi_h, \boldsymbol{z}_h, s_h)\|_{\boldsymbol{V}_2}} \Bigg).
\end{aligned}$$

From the above equation, and the definitions of bilinear forms $\mathbb{A}_2^h, \mathbb{A}_2, \mathbb{B}_2^h, \mathbb{B}_2$, we have

$$\begin{aligned}
&\|(\sigma_h, \boldsymbol{\tau}_h, \varrho_h)\|_{\boldsymbol{V}_2} \\
\lesssim &\sup_{(\psi_h, \boldsymbol{z}_h, s_h)\in \boldsymbol{V}_2^h} \frac{1}{\|(\psi_h, \boldsymbol{z}_h, s_h)\|_{\boldsymbol{V}_2}} \\
&\times \sum_{E\in\mathcal{T}_h} \Bigg(\big|\big((\boldsymbol{y}^s)_\pi - \boldsymbol{y}^s, \nabla\psi_h\big)_E\big| + \big|\big(\boldsymbol{\Pi}_{l,E}^0 \nabla(\varphi^s)_I - \nabla(\varphi^s)_I, \nabla\psi_h\big)_E - \big(\nabla(\varphi^s)_I - \nabla\varphi^s, \nabla\psi_h\big)\big| \\
&\qquad + \big|\big((\boldsymbol{y}^s)_\pi - \boldsymbol{y}^s, \nabla s_h\big)_E\big| + \big|\big(\nabla(\varphi^s)_I - \nabla\varphi^s, \boldsymbol{z}_h\big)_E + \big|\big((\boldsymbol{y}^s)_\pi - \boldsymbol{y}^s, \boldsymbol{z}_h\big)_E\big|\,\big| \\
&\qquad + \big|\big(\nabla(r^s)_I - \nabla r^s, \boldsymbol{z}_h\big)_E\big| + \big|\big(\Pi_{1,E}^0\varphi - \varphi, \psi_h\big)_E\big| + \big|\big(\Pi_{1,E}^0 r - r, \psi_h\big)_E\big| \\
&\qquad + \big|\big(\Pi_{1,E}^0\varphi - \varphi, s_h\big)_E\big| \Bigg) \\
\overset{(4.1),(4.4)}{\lesssim} &\; h^{\min\{\theta,1\}}\big(\|\varphi^s\|_{1+\theta} + \|\boldsymbol{y}^s\|_\theta + \|r^s\|_{1+\theta} + \|\varphi\|_1 + \|r\|_1\big) \\
\overset{(2.19)}{\lesssim} &\; h^{\min\{\theta,1\}}\|(\varphi, \boldsymbol{y}, r)\|_{\boldsymbol{V}_2}.
\end{aligned} \tag{4.11}$$

Combining (4.10), the above bound and applying the triangular inequality, we complete the proof of (4.6). □

Referring to the results in Theorem 4.1 and the definitions of the solution operators (4.5), we have the following convergence.

Corollary 4.1. *The convergence of the discrete solution operator $\boldsymbol{T}_2^h$ towards the continuous solution operator $\boldsymbol{T}_2$ holds true, furthermore,*

$$\big\|\boldsymbol{T}_2 - \boldsymbol{T}_2^h\big\|_{\mathcal{L}(\boldsymbol{V}_2)} \lesssim h^{\min\{\theta,1\}}, \tag{4.12}$$

where $\|\cdot\|_{\mathcal{L}(\boldsymbol{V}_2)}$ denotes the usual operator norm from $\boldsymbol{V}_2$ to $\boldsymbol{V}_2$.

Assuming that λ is an eigenvalue of (2.15) with algebraic multiplicity m and the ascent α, and $\lambda_h^1, \cdots, \lambda_h^m$ are enumerations of the approximate eigenvalues obtained by (3.13). Moreover, let $\mathcal{E}_\lambda$ denote the eigenspace related to the eigenvalue λ, and $\mathcal{E}_{\lambda,h}$ be the direct sum of the eigenspaces corresponding to $\lambda_h^1, \cdots, \lambda_h^m$. Given the two subspaces $\boldsymbol{X}, \boldsymbol{Y} \subseteq \boldsymbol{V}_2$, we denote

$$\delta(\boldsymbol{X}, \boldsymbol{Y}) := \sup_{\boldsymbol{x}\in\boldsymbol{X}, \|\boldsymbol{x}\|_{\boldsymbol{V}_2}=1} \Big(\inf_{\boldsymbol{y}\in\boldsymbol{Y}} \|\boldsymbol{x} - \boldsymbol{y}\|_{\boldsymbol{V}_2} \Big),$$

then the gap $\hat{\delta}$ between $\boldsymbol{X}$ and $\boldsymbol{Y}$ is defined by $\hat{\delta}(\boldsymbol{X}, \boldsymbol{Y}) := \max\{\delta(\boldsymbol{X}, \boldsymbol{Y}), \delta(\boldsymbol{Y}, \boldsymbol{X})\}$.

Theorem 4.2. *The following error estimates hold true:*

$$\hat{\delta}(\mathcal{E}_\lambda, \mathcal{E}_{\lambda,h}) \lesssim h^{\min\{\theta,1\}}, \quad \big|\lambda - \lambda_h^i\big| \lesssim h^{\frac{\min\{\theta,1\}}{\alpha}}, \quad \forall\, i = 1, \ldots, m. \tag{4.13}$$

Proof. By applying [7, Theorems 7.1 and 7.3], there are

$$\hat{\delta}(\mathcal{E}_\lambda, \mathcal{E}_{\lambda,h}) \lesssim \big\|\boldsymbol{T}_2 - \boldsymbol{T}_2^h\big\|_{\mathcal{L}(\boldsymbol{V}_2)}, \quad \big|\lambda - \lambda_h^i\big| \lesssim \big\|\boldsymbol{T}_2 - \boldsymbol{T}_2^h\big\|_{\mathcal{L}(\boldsymbol{V}_2)}^{\frac{1}{\alpha}}, \quad \forall\, i = 1, \ldots, m. \tag{4.14}$$

Inserting (4.12) into (4.14), we derive (4.13) directly. □

On the second step of the two-step approach for the convergence analysis of eigenvalue problems, we restrict to consider transmission eigenvalues with the ascent $\alpha = 1$ and then prove the finer error estimate for the stabilization-free VEM approximation.

Theorem 4.3. *Let λ and λ_h be respectively the eigenvalues of* (2.15) *and* (3.13) *associated to eigenfunctions $(\varphi, \boldsymbol{y}, r)$ and $(\varphi_h, \boldsymbol{y}_h, r_h)$ with $\|(\varphi, \boldsymbol{y}, r)\|_{\boldsymbol{V}_2} = \|(\varphi_h, \boldsymbol{y}_h, r_h)\|_{\boldsymbol{V}_2} = 1$, and λ^* and λ_h^* be respectively the eigenvalues of* (2.16) *and* (3.14) *associated to eigenfunctions $(\varphi^*, \boldsymbol{y}^*, r^*)$ and $(\varphi_h^*, \boldsymbol{y}_h^*, r_h^*)$ with $\|(\varphi^*, \boldsymbol{y}^*, r^*)\|_{\boldsymbol{V}_2} = \|(\varphi_h^*, \boldsymbol{y}_h^*, r_h^*)\|_{\boldsymbol{V}_2} = 1$. Assume the term $|\mathbb{B}_2((\varphi_h, \boldsymbol{y}_h, r_h), (\varphi_h^*, \boldsymbol{y}_h^*, r_h^*))|$ admits a positive lower bound uniformly with respect to h, then*

$$|\lambda - \lambda_h| \lesssim h^{2\min\{\theta,1\}}. \tag{4.15}$$

Proof. From (2.15), (2.16), (3.13), (3.14) and direct computation, we obtain

$$\begin{aligned}
&(\lambda_h - \lambda)\mathbb{B}_2\big((\varphi_h, \boldsymbol{y}_h, r_h), (\varphi_h^*, \boldsymbol{y}_h^*, r_h^*)\big) \\
&= \mathbb{A}_2\big((\varphi, \boldsymbol{y}, r) - (\varphi_h, \boldsymbol{y}_h, r_h), (\varphi^*, \boldsymbol{y}^*, r^*) - (\varphi_h^*, \boldsymbol{y}_h^*, r_h^*)\big) \\
&\quad - \lambda\mathbb{B}_2\big((\varphi, \boldsymbol{y}, r) - (\varphi_h, \boldsymbol{y}_h, r_h), (\varphi^*, \boldsymbol{y}^*, r^*) - (\varphi_h^*, \boldsymbol{y}_h^*, r_h^*)\big) \\
&\quad + \mathbb{A}_2^h\big((\varphi_h, \boldsymbol{y}_h, r_h), (\varphi_h^*, \boldsymbol{y}_h^*, r_h^*)\big) - \mathbb{A}_2\big((\varphi_h, \boldsymbol{y}_h, r_h), (\varphi_h^*, \boldsymbol{y}_h^*, r_h^*)\big) \\
&\quad + \lambda_h\left(\mathbb{B}_2\big((\varphi_h, \boldsymbol{y}_h, r_h), (\varphi_h^*, \boldsymbol{y}_h^*, r_h^*)\big) - \mathbb{B}_2^h\big((\varphi_h, \boldsymbol{y}_h, r_h), (\varphi_h^*, \boldsymbol{y}_h^*, r_h^*)\big)\right) \\
&=: I - II + III + IV.
\end{aligned} \tag{4.16}$$

By (4.13) and its corresponding adjoint result, the first two terms imply

$$|I - II| \lesssim \|(\varphi - \varphi_h, \boldsymbol{y} - \boldsymbol{y}_h, r - r_h)\|_{\boldsymbol{V}_2}\|(\varphi^* - \varphi_h^*, \boldsymbol{y}^* - \boldsymbol{y}_h^*, r^* - r_h^*)\|_{\boldsymbol{V}_2} \lesssim h^{2\min\{\theta,1\}}.$$

Further, we have the following bound:

$$\begin{aligned}
|III + IV| &\lesssim \sum_{E\in\mathcal{T}_h}\Big(\big|\big(\boldsymbol{\Pi}_{l,E}^0\nabla\varphi_h, \boldsymbol{\Pi}_{l,E}^0\nabla\varphi_h^*\big)_E - (\nabla\varphi_h, \nabla\varphi_h^*)_E\big| \\
&\qquad + \big|\big(\Pi_{1,E}^0\varphi_h, \Pi_{1,E}^0\varphi_h^*\big)_E - (\varphi_h, \varphi_h^*)_E\big| + \big|\big(\Pi_{1,E}^0 r_h, \Pi_{1,E}^0\psi_h^*\big)_E - (r_h, \psi_h^*)_E\big| \\
&\qquad + |(\Pi_{1,E}^0\varphi_h, \Pi_{1,E}^0 s_h^*)_E - (\varphi_h, s_h^*)_E|\Big) \\
&= \sum_{E\in\mathcal{T}_h}\Big(\big|\big(\boldsymbol{\Pi}_{l,E}^0\nabla\varphi_h - \nabla\varphi_h, \boldsymbol{\Pi}_{l,E}^0\nabla\varphi_h^* - \nabla\varphi_h^*\big)_E\big| + \big|\big(\Pi_{1,E}^0\varphi_h - \varphi_h, \Pi_{1,E}^0\varphi_h^* - \varphi_h^*\big)_E\big| \\
&\qquad + \big|\big(\Pi_{1,E}^0 r_h - r_h, \Pi_{1,E}^0\psi_h^* - \psi_h^*\big)_E\big| + \big|\big(\Pi_{1,E}^0\varphi_h - \varphi_h, \Pi_{1,E}^0 s_h^* - s_h^*\big)_E\big|\Big) \\
&\lesssim h^{2\min\{\theta,1\}}.
\end{aligned}$$

Inserting all the above estimates into (4.16), we conclude the proof of (4.15). □

Remark 4.1. Under the case of $n \neq 1$, one subtle point are hidden in the proof. Since the bilinear form $\mathbb{A}_1((\cdot,\cdot),(\cdot,\cdot))$ is not coercive over $\boldsymbol{V}_1$, it is natural to employ the $\mathbb{T}$-coercivity to close the corresponding theoretical analysis.

5. Numerical Results

In this section, we present numerical tests to demonstrate the validity of the stabilization-free VEM for the TEP on anisotropic media. In Section 5.1, we describe the process how to produce the generalized matrix eigenvalue problems. In Section 5.2, we present numerical tests to validate the theoretical results discussed in above section. Next, we provide motivations why to introduce the stabilization-free VEM for anisotropic TEP in Section 5.3. Eventually, the stabilization-free VEM is extended to high-order and high-dimensional cases in Section 5.4.

5.1. Matrix representation

The section is to present the matrix representation of the stabilization-free VEM schemes (3.9) and (3.13) to be implemented.

5.1.1. The case $n_* > \gamma > 1$ or $n^* < \gamma < 1$

We are in position to discuss the matrix formulation obtained by the stabilization-free VEM scheme (3.9). Let $V_{h,0}$ and $V_{h,b}$ denote the subspaces of V_h with vanishing boundary degrees of freedom and vanishing internal degrees of freedom, respectively. Since $(w_h, u_h) \in \boldsymbol{V}_1^h$ in (3.9), where requires the constraint condition $w_h - u_h = 0$ on the boundary $\partial\Omega$, we enforce the boundary condition by explicitly taking

$$w_h = w_{h,0} + w_{h,b}, \quad u_h = u_{h,0} + w_{h,b}, \quad w_{h,0}, u_{h,0} \in V_{h,0}, \quad w_{h,b} \in V_{h,b}.$$

Then we have

- by taking $\psi_h = \psi_{h,0} \in V_{h,0}$ and $s_h = 0$ in (3.9),

$$a_h^{\boldsymbol{A}}(w_{h,0} + w_{h,b}, \psi_{h,0}) - c_h\big(n(w_{h,0} + w_{h,b}), \psi_{h,0}\big) = \lambda_h c_h\big(n(w_{h,0} + w_{h,b}), \psi_{h,0}\big),$$

- by taking $\psi_h = 0$ and $s_h = s_{h,0} \in V_{h,0}$ in (3.9),

$$-a_h\big((u_{h,0} + w_{h,b}), s_{h,0}\big) - c_h\big((u_{h,0} + w_{h,b}), s_{h,0}\big) = -\lambda_h c_h(u_{h,0} + w_{h,b}, s_{h,0}),$$

- by taking $\psi_h = s_h = \psi_{h,b} \in V_{h,b}$ in (3.9),

$$\begin{aligned} &a_h^{\boldsymbol{A}}(w_{h,0} + w_{h,b}, \psi_{h,b}) + c_h\big(n(w_{h,0} + w_{h,b}), \psi_{h,b}\big) \\ &\quad - a_h(u_{h,0} + w_{h,b}, \psi_{h,b}) - c_h(u_{h,0} + w_{h,b}, \psi_{h,b}) \\ &= \lambda_h\big[c_h\big(n(w_{h,0} + w_{h,b}), \psi_{h,b}\big) - c_h(u_{h,0} + w_{h,b}, \psi_{h,b})\big]. \end{aligned}$$

Let $\{\xi_i\}_{i=1}^N$ be a basis of the stabilization-free virtual element space V_h, $\{\xi_i^0\}_{i=1}^{N_0}$ be a basis of the space $V_{h,0}$, and $\{\xi_i^b\}_{i=1}^{N_b}$ be a basis of the space $V_{h,b}$, respectively. For $\xi_i, \xi_j \in V_h$ $(1 \le i, j \le N)$, we write

$$S_{\boldsymbol{A}} := a_h^{\boldsymbol{A}}(\xi_i, \xi_j), \quad S := a_h(\xi_i, \xi_j), \quad M_n := c_h(n\xi_i, \xi_j), \quad M := c_h(\xi_i, \xi_j).$$

Upon that we obtain the generalized eigenvalue problem

$$\mathcal{A}_1 \boldsymbol{w} = \lambda_h \mathcal{M}_1 \boldsymbol{w}, \tag{5.1}$$

where the vector $\boldsymbol{w}$ is given by $\boldsymbol{w} = (w_{h,0}, u_{h,0}, w_{h,b})^\intercal$, and the matrices $\mathcal{A}_1$ and $\mathcal{M}_1$ are defined by

$$\mathcal{A}_1 = \begin{pmatrix} (S_{\boldsymbol{A}} + M_n)^{N_0\times N_0} & 0 & (S_{\boldsymbol{A}} + M_n)^{N_0\times N_b} \\ 0 & -(S+M)^{N_0\times N_0} & -(S+M)^{N_0\times N_b} \\ (S_{\boldsymbol{A}} + M_n)^{N_b\times N_0} & -(S+M)^{N_b\times N_0} & (S_{\boldsymbol{A}}+M_n-S-M)^{N_b\times N_b} \end{pmatrix}_{(2N_0+N_b)\times(2N_0+N_b)},$$

$$\mathcal{M}_1 = \begin{pmatrix} M_n^{N_0\times N_0} & 0 & M_n^{N_0\times N_b} \\ 0 & -M^{N_0\times N_0} & -M^{N_0\times N_b} \\ M_n^{N_b\times N_0} & -M^{N_b\times N_0} & M_n^{N_b\times N_b} - M^{N_b\times N_b} \end{pmatrix}_{(2N_0+N_b)\times(2N_0+N_b)}.$$

5.1.2. The case $n \equiv 1$

Recalling that $\{\xi_i\}_{i=1}^{N}$ is a basis of V_h, $\{\xi_i^0\}_{i=1}^{N_0}$ is a basis of $V_{h,0}$ and

$$S_{\boldsymbol{A}} := a_h^{\boldsymbol{A}}(\xi_i, \xi_j), \quad M := c_h(\xi_i, \xi_j), \quad 1 \le i, j \le N.$$

Moreover, the solutions φ_h and r_h in the scheme (3.12) have zero mean values over Ω : $(\varphi_h, 1)$=0 and $(r_h, 1) = 0$. We denote the vectors α and β as

$$\alpha := \big((\xi_1^0, 1), (\xi_2^0, 1), \cdots, (\xi_{N_0}^0, 1)\big), \quad \beta := \big((\xi_1, 1), (\xi_2, 1), \cdots, (\xi_N, 1)\big).$$

Following the processing to the problem (2.14) in recent work [42, Section 4], the stabilization-free VEM scheme (3.13) can provide the matrix representation

$$\mathcal{A}_2 \boldsymbol{\varphi} = \lambda_h \mathcal{M}_2 \boldsymbol{\varphi}, \tag{5.2}$$

where the eigenvector $\boldsymbol{\varphi} := (\varphi_h, r_h, \sigma, \tau)$ (σ, τ are the auxiliary Lagrangian multipliers associated to α and β) and

$$\mathcal{A}_2 = \begin{pmatrix} S_{\boldsymbol{A}}^{N_0\times N_0} & S_{\boldsymbol{A}}^{N_0\times N} & \alpha & 0 \\ S_{\boldsymbol{A}}^{N\times N_0} & S_{\boldsymbol{A-I}}^{N\times N} & 0 & \beta \\ \alpha^T & 0 & 0 & 0 \\ 0 & \beta^T & 0 & 0 \end{pmatrix}_{2(N_0+N)\times 2(N_0+N)},$$

$$\mathcal{M}_2 = \begin{pmatrix} M^{N_0\times N_0} & M^{N_0\times N} & 0 & 0 \\ M^{N\times N_0} & 0 & 0 & 0 \\ 0 & 0 & 0 & 0 \\ 0 & 0 & 0 & 0 \end{pmatrix}_{2(N_0+N)\times 2(N_0+N)}.$$

Since $\mathcal{A}_i$ and $\mathcal{M}_i$ $(i = 1, 2)$ are symmetric matrices, thus, we can employ the MATLAB function `eigs` to compute the matrix eigenvalue problems (5.1) and (5.2).

5.2. Theoretical validation

After the above preparation, we implement numerical experiments to validate the theoretical results in the main Theorem 4.3 for the two cases $n \neq 1$ and $n \equiv 1$ separately.

5.2.1. The case $n_* > \gamma > 1$

In Sections 5.2.1 and 5.2.2, the computational domain is fixed as the square domain $\Omega_S = [0, 1]^2$, which is decomposed by the four families of meshes, as shown in Fig. 5.1: square mesh $\mathcal{T}_h^1$, hexagonal mesh $\mathcal{T}_h^2$, concave mesh $\mathcal{T}_h^3$; adding the middle point on each edge of mesh $\mathcal{T}_h^2$ to generate mesh $\mathcal{T}_h^4$; meanwhile, $\mathcal{T}_h^4$ also incorporates a distortion having a more complex element geometry.

The mesh size is set to h_i with $i = 1, 2, 3, 4$. From Theorem 4.3, the theoretical convergence rate of the approximated transmission eigenvalue is $\mathcal{O}(h^2)$ with respect to the mesh size h, which is equivalent to $\mathcal{O}(N^{-1})$ as the total number N of degrees of freedom increases. To measure the convergence rate, we compute the relative error quantity $\mathrm{Error}(h_{i+1}) = |(k_{h_i} - k_{h_{i+1}})/k_{h_{i+1}}|$,

where k_{h_i} denotes the computed transmission eigenvalue obtained by the stabilization-free VEM on the mesh of size h_i. Visually, we apply MATLAB function `loglog` to depict error curves in plot.

The configurations are given by

$$\boldsymbol{A}(x,y) = \begin{pmatrix} 2+x^2 & xy \\ xy & 2+y^2 \end{pmatrix} \quad \text{and} \quad n(x,y) = 4 + 2(x+y), \quad (x,y) \in \Omega_S.$$

Some representative numerical results of the first four real transmission eigenvalues are collected into Tables 5.1 and 5.2 with $l = 0, 1, 2$. These values are consistent with the reference solutions in [56, Table 3] calculated by the multilevel correction method. Moreover, we plot the relative errors in Figs. 5.2 and 5.3.

As previous assumptions, for any polygonal element E, the stabilization-free VEM scheme is valid by choosing $l \in \mathbb{N}$ to satisfy the sufficient condition (3.7), that is, for $l = 0$, the stabilization-free VEM scheme on any polygon that is not a triangle will give bad results; for $l = 1$, the restricted maximum vertex number is 5. It can be seen from Figs. 5.2(a) and 5.2(d) that some spurious transmission eigenvalues appear once violating sufficient condition

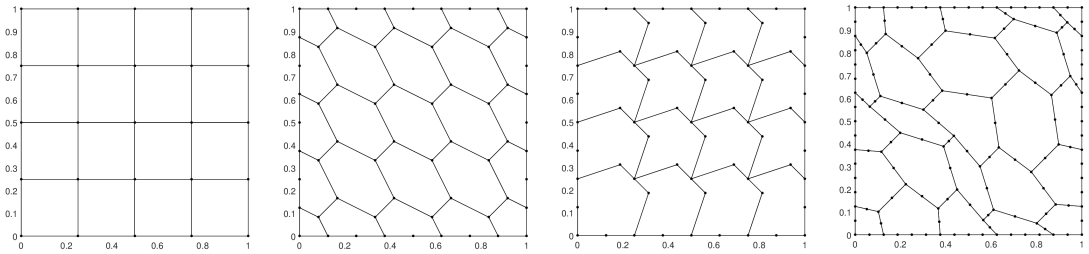

(a) $\mathcal{T}_h^1, \max(N_E^V) = 4$ (b) $\mathcal{T}_h^2, \max(N_E^V) = 6$ (c) $\mathcal{T}_h^3, \max(N_E^V) = 8$ (d) $\mathcal{T}_h^4, \max(N_E^V) = 12$

Fig. 5.1. Test 5.2.1: Sample meshes on Ω_S.

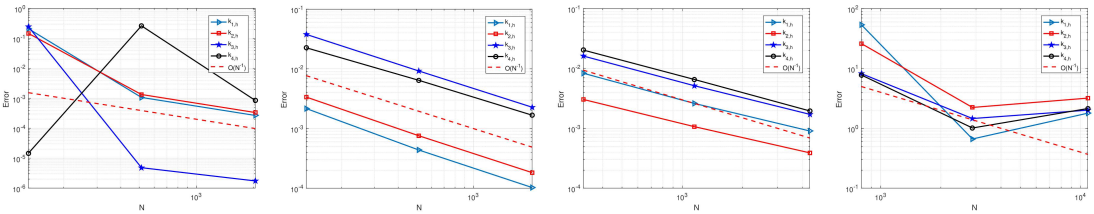

(a) $\mathcal{T}_h^1$, $l = 0$ (b) $\mathcal{T}_h^1$, $l = 1$ (c) $\mathcal{T}_h^2$, $l = 1$ (d) $\mathcal{T}_h^4$, $l = 1$

Fig. 5.2. Test 5.2.1: Relative errors of the first four real transmission eigenvalues ($l = 0, 1$).

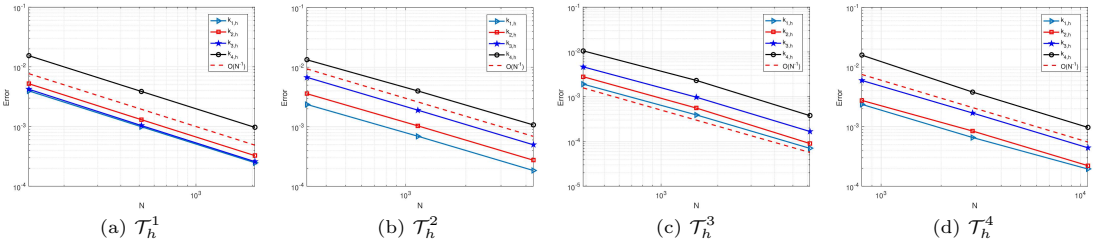

(a) $\mathcal{T}_h^1$ (b) $\mathcal{T}_h^2$ (c) $\mathcal{T}_h^3$ (d) $\mathcal{T}_h^4$

Fig. 5.3. Test 5.2.1: Relative errors of the first four real transmission eigenvalues ($l = 2$).

Table 5.1: Test 5.2.1: The first four real transmission eigenvalues on Ω_S ($n \neq 1$ and $l = 0, 1$).

l	Mesh	N	$k_{1,h}$	$k_{2,h}$	$k_{3,h}$	$k_{4,h}$
0	$\mathcal{T}_h^1$	130	1.1697616472	1.4891990369	1.7549439410	2.3339457709
		514	1.4828760836	1.7456061960	2.3339797360	2.3339797360
		2050	1.4812942786	1.7432750766	2.3339685158	3.1670532273
		8194	1.4808987741	1.7426925226	2.3339644590	3.1643715194
1	$\mathcal{T}_h^1$	130	1.4848200584	1.7501144129	2.4520042215	3.2629744968
		514	1.4816158562	1.7442405185	2.3626249600	3.1909483210
		2050	1.4809695899	1.7429212801	2.3410475425	3.1705721310
		8194	1.4808174686	1.7426031943	2.3357278637	3.1652700423
	$\mathcal{T}_h^2$	320	1.4993281088	1.7509745757	2.3907687265	3.7338447360
		1152	1.4869387054	1.7456707332	2.3527401794	3.6869094589
		4352	1.4830751698	1.7438124498	2.3406891967	3.1729593108
		16896	1.4817372385	1.7431336768	2.3366845706	3.1667735589
	$\mathcal{T}_h^4$	800	0.1041373152	0.1546667444	0.1707046380	0.1738765251
		2880	0.0018943922	0.0056975732	0.0185054946	0.0197679047
		10880	0.0011386101	0.0017618717	0.0075279044	0.0098189547
		42240	0.0004078151	0.0004195823	0.0024986901	0.0031256425

Table 5.2: Test 5.2.1: The first four real transmission eigenvalues on Ω_S ($n \neq 1$ and $l = 2$).

Mesh	N	$k_{1,h}$	$k_{2,h}$	$k_{3,h}$	$k_{4,h}$
$\mathcal{T}_h^1$	130	1.4885873338	1.7546284742	2.3470575391	3.2287815254
	514	1.4827223222	1.7455254280	2.3371931583	3.1798213562
	2050	1.4812559550	1.7432547654	2.3347677613	3.1675643247
	8194	1.4808892230	1.7426874364	2.3341640049	3.1644985082
$\mathcal{T}_h^2$	320	1.4856690052	1.7512011191	2.3557830589	3.2230552393
	1152	1.4821570544	1.7449408451	2.3399504847	3.1806786127
	4352	1.4811331722	1.7431403102	2.3355221970	3.1680457346
	16896	1.4808608240	1.7426625225	2.3343604344	3.1646507676
$\mathcal{T}_h^3$	386	1.4843149667	1.7484930702	2.3475813159	3.2058653178
	1538	1.4814837848	1.7436171664	2.3367189756	3.1722784510
	6146	1.4809039356	1.7426457027	2.3344439996	3.1649648496
	24578	1.4807998519	1.7424888175	2.3340533709	3.1637693968
$\mathcal{T}_h^4$	800	1.4856280153	1.7492797565	2.3532142247	3.2300385884
	2880	1.4821258384	1.7444731089	2.3392862171	3.1797189796
	10880	1.4811543766	1.7430052302	2.3353400956	3.1677045694
	42240	1.4808661922	1.7426190226	2.3343080109	3.1646304770

(3.7), meanwhile, Fig. 5.2(c) tells us that the optimal convergence order may be also destroyed, where its behavior is actually lower than the optimal convergence rate $\mathcal{O}(N^{-1})$ slightly in this case (resemble results obtained for the mesh $\mathcal{T}_h^3$ are not reported here).

By lifting the value of l, i.e. $l = 2$, good numerical results in Table 5.2 and Fig. 5.3 are recovered independently of the used meshes and some observations are concluded as follows. Along with increasing degrees of freedom, the computational transmission eigenvalues are decreasing with the optimal convergence order, which is consistent with the theoretical result in Theorem 4.3. On the other hand, we stress from Fig. 5.3(d) that the condition (3.7) is only sufficient but not strictly necessary. Special care and other techniques to introduce the stabilization-free VEM are still required.

5.2.2. The case $n \equiv 1$

In this subsection, we report in Tables 5.3-5.4 the numerical results for (1.1) with the matrix $\boldsymbol{A} = (1/4)\boldsymbol{I}$ and the index of refraction $n \equiv 1$, where the example is taken from [37].

All observations are summarized as follows. For all the used meshes, numerical results of the stabilization-free VEM are closer and closer to the reference eigenvalues from above when the total number of degrees of freedom ascends. Meanwhile, it attains the theoretical convergence order $\mathcal{O}(N^{-1})$. In particular, noticing that the stabilization-free VEM with $l = 1$ using the mesh $\mathcal{T}_h^4$ can not find real eigenvalues, since it violates the sufficient condition (3.7) badly and produces wrong numerical results. As expected, the optimal performance of the stabilization-free VEM is presented in Table 5.4 by improving $l = 2$.

5.2.3. Stratified domain

In this section, we consider the much interesting case of the TEP on the stratified medium. As a simple test, we here investigate two layer medium, and the numerical method can also

Table 5.3: Test 5.2.2: The first four real transmission eigenvalues on Ω_S ($n \equiv 1$ and $l = 1$).

Mesh	N	$k_{1,h}$	$k_{2,h}$	$k_{3,h}$	$k_{4,h}$
$\mathcal{T}_h^1$	132	6.9803719445	8.3815661660	8.3815661660	10.316388996
	516	5.7020572871	6.5668387404	6.5668387404	7.3495954853
	2052	5.3880069730	6.1469150387	6.1469150387	6.6407777817
	8196	5.3204181162	6.0387002978	6.0387002978	6.4706578202
	Order	-1.103605047	-0.969380186	-0.969380186	-1.014980313
$\mathcal{T}_h^2$	322	5.9598624545	6.4698735776	7.2168385874	8.2455640789
	1154	5.4577803400	6.1227775021	6.3515980583	6.7639062165
	4354	5.3388793015	6.0325855682	6.0917448923	6.4997685363
	16898	5.3086854666	6.0095717146	6.0245540098	6.4355534182
	Order	-1.027955842	-1.025726057	-1.010262570	-1.057568002
$\mathcal{T}_h^3$	388	5.5732006833	6.2401873659	6.4628131357	6.9019270584
	1540	5.3671130510	6.0716548059	6.1371480489	6.5645932303
	6148	5.3160424481	6.0204077603	6.0380807816	6.4545607423
	24580	5.3030842808	6.0069534782	6.0114523622	6.4247086458
	Order	-0.988946268	-0.964444430	-0.945863040	-0.938989530
$\mathcal{T}_h^4$	–	–	–	–	–

Table 5.4: Test 5.2.2: The first four real transmission eigenvalues on Ω_S ($n \equiv 1$ and $l = 2$).

Mesh	N	$k_{1,h}$	$k_{2,h}$	$k_{3,h}$	$k_{4,h}$
$\mathcal{T}_h^1$	132	5.8237530993	7.2115028445	6.6586374471	6.6586374471
	516	5.4142273581	6.1488048583	6.1488048583	6.5890980778
	2052	5.3267131992	6.4566718058	6.0380570229	6.0380570229
	8196	5.3055657630	6.0111763311	6.4249406700	6.0111763311
	Order	-1.025962659	-1.022399979	-1.022399979	-1.031393529
$\mathcal{T}_h^2$	322	5.7453467111	6.3283000618	6.8822469320	7.3826256124
	1154	5.4041018552	6.0867277116	6.2176264442	6.6151654593
	4354	5.3247844727	6.0236424472	6.0557392521	6.4642631010
	16898	5.3051322079	6.0076462565	6.0156570346	6.4269750595
	Order	-1.047976696	-1.031341167	-1.046288953	-1.048434663
$\mathcal{T}_h^3$	388	5.6436089902	6.4556881222	6.5261613312	7.0691583210
	1540	5.3726509321	6.1064823047	6.1095138293	6.5552990551
	6148	5.3161840513	6.0265753325	6.0275540490	6.4471291211
	24580	5.3029067722	6.0081392546	6.0085246343	6.4224023764
	Order	-1.043887194	-1.057171744	-1.052542015	-1.063301385
$\mathcal{T}_h^4$	802	5.8169268220	6.4183879719	6.8327562054	7.2237885272
	2882	5.4160762714	6.1124264357	6.2066745923	6.6164012049
	10882	5.3263465562	6.0296672690	6.0497095202	6.4635081773
	42242	5.3054093631	6.0091057352	6.0138833843	6.4266895642
	Order	-1.092359102	-1.045514183	-1.107464827	-1.067285160

be generalized to the stratified domain with more than two layers. We still take $\boldsymbol{A} = (1/4)\boldsymbol{I}$ and the index of refraction $n \equiv 1$ on the unit disk Ω_D with the center $(0, 0)$, which contains a concenteric disk with radius $r = 0.1$ inside, whose reference solutions refer to [36].

As depicted in Fig. 5.4, we select two types of meshes, namely triangular mesh $\mathcal{T}_h$ and Voronoi mesh $\mathcal{V}_h$. The Voronoi mesh is created by the PolyMesher package in [52]. With the stabilization-free VEM with $l = 2$, the computed first four real transmission eigenvalues are reported in Table 5.5. Each column of the table shows that the method converges to the exact eigenvalues from above with respect to space discretization. Moreover, the convergence orders of the relative errors on the two sequence of meshes are expected to be the optimal.

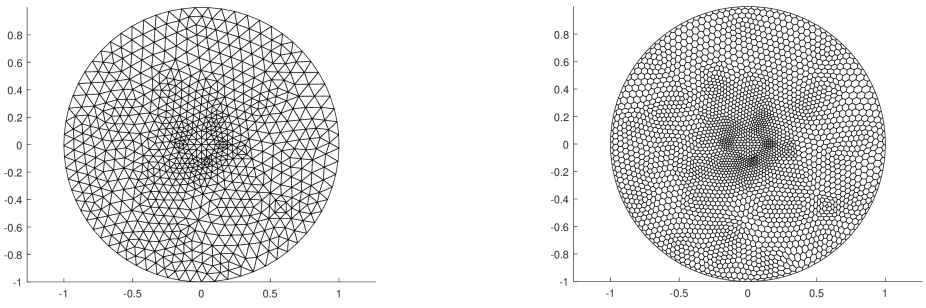

(a) $\mathcal{T}_h$ (b) $\mathcal{V}_h$

Fig. 5.4. Test 5.2.3: A schematic of the sample meshes on the stratified domain.

Table 5.5: Test 5.2.3: The first four real transmission eigenvalues on Ω_D ($n \equiv 1$ and $l = 2$).

Mesh	N	$k_{1,h}$	$k_{2,h}$	$k_{3,h}$	$k_{4,h}$
$\mathcal{T}_h$	366	2.9958912518	3.5414676942	3.5458829012	4.0621802579
	1452	2.9261684201	3.4364517298	3.4373207060	3.8551017824
	5796	2.9085260096	3.4094668464	3.4096646227	3.8011841878
	23172	2.9040901172	3.4026570430	3.4027049448	3.7875478492
	Order	-0.995037497	-0.992052982	-0.994040822	-0.989318762
$\mathcal{V}_h$	506	3.0175477003	3.5613925553	3.5866568297	4.0786330146
	1924	2.9313925553	3.4400481669	3.4466732358	3.8554678509
	7549	2.9108297269	3.4118731598	3.4134284834	3.8032724722
	29575	2.9055986330	3.4047196232	3.4049184789	3.7917740574
	Order	-1.000041767	-1.001258832	-0.994988690	-1.104423732

In conclusion, these experiments in Section 5.2 confirm the theoretical prediction of Theorem 4.3 and particularly, identify the influence of the parameter l related to the shape of polygonal elements.

5.3. The virtues of the stabilization-free VEM

5.3.1. Particular advantages of the stabilization-free VEM for eigenvalue problems

From the theoretical point of view, as shown in [34], the possible choices of VEM bilinear forms on the right-hand side contain non-stabilized and stabilized ones. To derive the convergence, both VEM schemes appeal for different theoretical frameworks: the spectral approximation theory of compact operators from Babuška and Osborn [7] and the other one of noncompact operators from Descloux, Nassif and Rappaz [32]. It is clear that the convergence analysis for the stabilization-free VEM of spectral problems can be simply completed by the spectral approximation theory of compact operators.

Besides, as for the TEP with $n \equiv 1$ peculiarly dealt here, see Section 3.3, if we consider the standard VEM scheme with stabilizations, the VEM scheme shall be more complex than the scheme (3.12). For example, in order to show the well-posed property of the discrete solution operator $\boldsymbol{T}_2^h$, we must prove the inf-sup condition (3.19), which is also required in the error estimates. Other than standard change for the discrete bilinear form $a_h(\cdot\,,\cdot)$, we also have to add new terms $S((I-\Pi_1^\nabla)r_h,(I-\Pi_1^\nabla)r_h)$ in (3.12b) and $S((I-\Pi_1^\nabla)s_h,(I-\Pi_1^\nabla)s_h)$ in (3.12c) to complete the proof apparently, where the symmetric bilinear form $S(\cdot\,,\cdot)$ is a standard stabilization term of the VEM, referring to [8]. Indeed, for given $r_h \in \hat{V}_h$ and setting $\boldsymbol{z}_h = -\nabla\Pi_1^\nabla r_h \in [\mathbb{P}_0(\Omega)]^2$, we get

$$\begin{aligned}
&-\big(\nabla\Pi_1^\nabla r_h,\boldsymbol{z}_h\big)+S\big((I-\Pi_1^\nabla)r_h,(I-\Pi_1^\nabla)r_h\big)\\
&\gtrsim \big\|\nabla\Pi_1^\nabla r_h\big\|_0^2+\big\|\nabla(I-\Pi_1^\nabla)r_h\big\|_0^2\\
&\gtrsim \|\boldsymbol{z}_h\|_0\|\nabla r_h\|_0,
\end{aligned}$$

which, together with the Poincaré inequality, derives the following inf-sup condition:

$$\sup_{(\psi_h,\boldsymbol{z}_h)\in\hat{V}_{h,0}\times[\mathbb{P}_0(\Omega)]^2}\frac{-\big(\nabla\Pi_1^\nabla r_h,\boldsymbol{z}_h\big)+S\big((I-\Pi_1^\nabla)r_h,(I-\Pi_1^\nabla)r_h\big)}{\|\psi_h\|_1+\|\boldsymbol{z}_h\|_0}\gtrsim\|r_h\|_1. \tag{5.3}$$

This makes at the price of more cumbersome techniques, which we prefer to avoid. In turn, the stabilization-free VEM scheme (3.12) is easier to understand and to complete the theoretical analysis.

From the numerical perspective, as highlighted by Boffi *et al.* [20] and discussed by Meng *et al.* [46], the stabilization parameters on both sides of the original VEM schemes of eigenvalue problems have dramatic effects on the VEM performance. As a consequence, there needs lots of arguments for stabilization parameters to provide well approximation of eigenvalue problems [14,20,34,41,46,47]. By virtue of the stabilization-free VEM, we remove all stabilization terms and then special treatments are not needed. The benefit is clearly appreciated and left to the interested reader to demonstrate.

Moreover, the monotonicity of approximating exact eigenvalue is an interesting topic [6,33]. As we know, the conforming finite element methods of elliptic eigenvalue problems yield the upper bound of exact eigenvalues by the min-max principle [6]. However, such VEM schemes guaranteed error bounds have not been considered, since different stabilization terms and meshes affect the numerical performance [14, 34, 47]. The stabilization-free VEM to solve eigenvalue problems seems to obtain good approximation for exact eigenvalues from above independently of meshes, please check Tables 5.1-5.5.

5.3.2. Strongly anisotropic case

The another advantage of the proposed stabilization-free VEM scheme is that the absence of the stabilization terms can reduce the error in case of anisotropic problems [17], since the stabilization terms raise an isotropic component of the error [5]. In particular, the present test is to show the potential advantage for the anisotropic TEP.

To this end, we compare the stabilization-free VEM ($l = 2$) with the standard VEM having `dofi-dofi` stabilization terms in [44] for the TEP on anisotropic media. Here the index of refraction $n(x, y)$ is taken as 4 and the strongly anisotropic structure is reflected by the matrix

$$\boldsymbol{A}(x, y) = 8 \cdot 10^{-3}\big(e_1 e_1^T\big) + \big(e_2 e_2^T\big),$$

where e_1 and e_2 are the vectors of the canonical basis of $\mathbb{R}^2$. Among all the scatterers $\mathcal{D}_1$-$\mathcal{D}_4$ shown in Fig. 5.5, we decompose them by a sequence of Voronoi meshes and compute the first real transmission eigenvalue by the stabilization-free VEM ($l = 2$) and standard VEM, respectively, see Table 5.6. To observe the magnitude of the error, we calculate the transmission

Table 5.6: Test 5.3.2: The smallest transmission eigenvalue obtained by the stabilization-free VEM (in short, SVEM) and standard VEM (in short, VEM) on different scattering shapes.

Method	N	$k_{h,\mathcal{D}_1}$	$k_{h,\mathcal{D}_2}$	$k_{h,\mathcal{D}_3}$	$k_{h,\mathcal{D}_4}$
SVEM	757	1.1237208411	1.0906778472	1.0811221347	1.1121316016
	1539	1.0790990217	1.0626595377	1.0556612327	1.0833265384
	3114	1.0543899636	1.0462007306	1.0429029653	1.0678957840
	6267	1.0343861047	1.0363411893	1.0341121946	1.0566513307
VEM	757	1.1423222115	1.1174949191	1.1038656352	1.1403830941
	1539	1.0858915747	1.0767895132	1.0681702195	1.0978029776
	3114	1.0568600424	1.0549308931	1.0499893883	1.0755284419
	6267	1.0364460060	1.0409516067	1.0379847644	1.0605922483

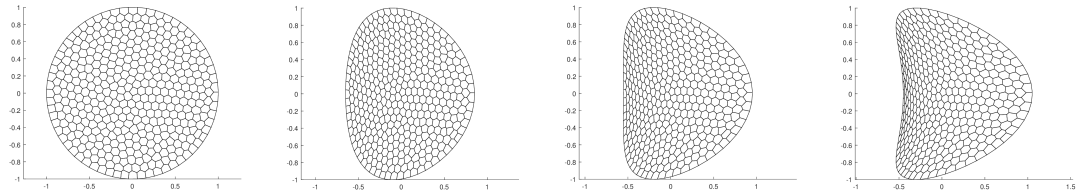

(a) $\mathcal{D}_1$ (b) $\mathcal{D}_2$ (c) $\mathcal{D}_3$ (d) $\mathcal{D}_4$

Fig. 5.5. Test 5.3.2: A variety of scatterers decomposed by Voronoi meshes.

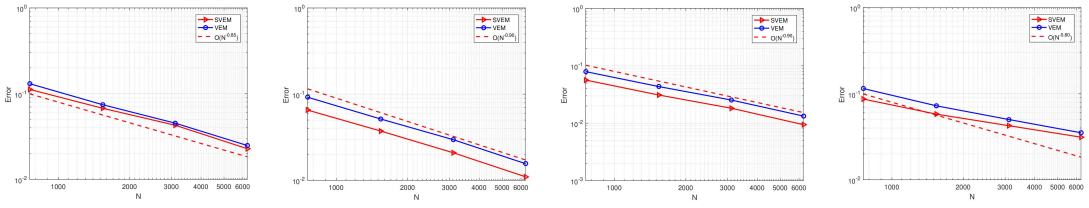

(a) $\mathcal{D}_1$ (b) $\mathcal{D}_2$ (c) $\mathcal{D}_3$ (d) $\mathcal{D}_4$

Fig. 5.6. Test 5.3.2: Errors of the first real transmission eigenvalue obtained by the stabilization-free VEM and standard VEM on different scattering shapes.

eigenvalues by the finite element method with 66882 degrees of freedom on the triangular mesh as reference values

$$k_{\mathcal{D}_1} = 1.01157777, \quad k_{\mathcal{D}_2} = 1.02536406, \quad k_{\mathcal{D}_3} = 1.02470023, \quad k_{\mathcal{D}_4} = 1.04428055.$$

Fig. 5.6 displays the behaviour of the error (computed by $\text{Error} = k_{h,\mathcal{D}_i} - k_{\mathcal{D}_i}$, $i = 1, 2, 3, 4$) obtained by the two methods. We observe the same trend of convergence curves. Since the regularity index of the associated eigenfunction is lower than one due to the strong anisotropy $\boldsymbol{A}$, then the convergence rate is determined by the regularity of the associated eigenspace. The observation also verifies the theory in Theorem 4.3. Moreover, the adaptive VEM scheme is able to recover the optimal convergence of the approximate eigenvalues, for example, see [44, 54], while the stabilization-free adaptive VEM of the TEP will be a future subject.

Especially, from Fig. 5.6, the magnitude of the error done by the stabilization-free VEM is less than the one obtained by the standard VEM under the anisotropic case, since the stabilization is an isotropic operator, adding the error of isotropic part regardless of the nature of the anisotropic problem.

All in all, the stabilization-free VEM is a very powerful tool to compute transmission eigenvalues on anisotropic materials.

5.4. High-order and high-dimensional stabilization-free VEM

In the forthcoming, we present the numerical extensions of the stabilization-free VEM and show the robustness of the proposed method on more general cases.

5.4.1. High-order stabilization-free VEM

Inspired by existing works [15, 26], we are interested in the higher-order stabilization-free VEM

for the TEP on anisotropic media. From [15], the sufficient condition (3.7) is enhanced by

$$(\ell+l)(\ell+l+1) \geq \ell N_E^V + \ell(\ell+1) - 3, \tag{5.4}$$

where ℓ denotes the degree of accuracy of the following high-order enlarged enhancement virtual element space, that is, the generalization of the lowest-order case (3.2),

$$V_h^\ell(E) = \Big\{ v_h \in H^1(E) \cap C^0(\partial E) \ : v_h|_e \in \mathbb{P}_\ell(e),\ \forall\, e \in \partial E,\ \Delta v_h \in \mathbb{P}_{\ell+l}(E), \\ \int_E (v_h - \Pi_{\ell,E}^\nabla v_h) p \mathrm{d}E = 0,\ \forall\, p \in \mathbb{P}_{(\ell+l)/(\ell-2)}(E) \Big\}.$$

The degrees of freedom are assigned by [2, 15]

(V_{D1}) the values of v_h at all vertices of the polygonal element E,

(V_{D2}) the values of v_h at $(\ell-1)$ internal Gauss-Lobatto nodes on each edge $e \in \partial E$,

(V_{D3}) the moments of v_h on element E: $(v_h, p_{\ell-2})_E$ for any $p_{\ell-2} \in \mathbb{P}_{\ell-2}(E)$.

For any matrix $\boldsymbol{M} \in \mathbb{R}^{2\times 2}$, any elements $u_h, v_h \in V_h^\ell(E)$, the discrete bilinear forms on the element level are introduced by

$$\begin{aligned} a_{h,\ell}^{\boldsymbol{M},E}(u_h, v_h) &= \big(\boldsymbol{M}\boldsymbol{\Pi}_{\ell+l-1,E}^0 \nabla u_h, \boldsymbol{\Pi}_{\ell+l-1,E}^0 \nabla v_h\big)_E, c_{h,\ell}^E(u_h, v_h) \\ &= \big(\Pi_{\ell,E}^0 u_h, \Pi_{\ell,E}^0 v_h\big)_E. \end{aligned}$$

Similarly, the global stabilization-free VEM bilinear forms can be defined by adding all local terms. Then we can similarly discretize (2.3) by the stabilization-free VEM scheme (3.9) of general order.

Remark 5.1. In this subsection, we only focus on the case $n_* > \gamma > 1$, and the higher-order extension of the other case $n \equiv 1$ is also easy to be considered, which is not reported repetitively. Note that all the stabilization terms have been removed, which leads that the stability analysis is very complicated. The proof of the well-posedness for the lowest-order stabilization-free VEM schemes of the Poisson problem and the linear elasticity problem can be found in [16, 27], then their extensions to higher-order cases are investigated in [15, 26], respectively.

Remark 5.2. As is known, the number of degrees of freedom for the VEM is bigger than the Lagrange finite element method. On the one hand, static condensation as for the finite element method can be applied to accelerate the computational efficiency of the high-order stabilization-free VEM. On the other hand, the serendipity techniques in [13] can also be incorporated into stabilization-free VEM to reduce degrees of freedom [26].

Here we contain a new configuration

$$\boldsymbol{A}(x,y) = \begin{pmatrix} 1/8 & 0 \\ 0 & 1/2 \end{pmatrix} \quad \text{and} \quad n(x,y) = 4, \quad (x,y) \in \Omega_S^{'} := [-0.5, 0.5]^2.$$

This example is taken from [39], where the method of fundamental solution loses high accuracy on the scatterer shape with corners (for example, the domain $\Omega_S^{'}$) and computes the first four real transmission eigenvalues as

$$k_{1,h} = 1.998, \quad k_{2,h} = 2.021, \quad k_{3,h} = 2.798, \quad k_{4,h} = 2.853.$$

The domain $\Omega_S^{'}$ is subdivided by the same polygonal meshes $\mathcal{T}_h^1, \mathcal{T}_h^2, \mathcal{T}_h^3$, and $\mathcal{T}_h^4$ in Fig. 5.1. Numerical results are presented in Table 5.7 for the fixed $\ell = 2$ and $l = 3$. From Table 5.7, the present algorithm is able to compute the transmission eigenvalues with higher accuracy than the computation executed by the method of fundamental solution [39]. Meanwhile, the optimal convergence order $\mathcal{O}(N^{-2})$ is observed when the degree of accuracy $\ell = 2$. Analogous results of high-order stabilization-free VEM were obtained for the tests in Section 5.2 (not reported).

Table 5.7: Test 5.4.1: The first four real transmission eigenvalues on $\Omega_S^{'}$ with $\ell = 2$ ($n \neq 1$ and $l = 3$).

Mesh	N	$k_{1,h}$	$k_{2,h}$	$k_{3,h}$	$k_{4,h}$
$\mathcal{T}_h^1$	514	2.0034820835	2.0266560211	2.8326019600	2.8962447902
	2050	1.9979291285	2.0209377580	2.8000046113	2.8558739497
	8194	1.9975144454	2.0205446924	2.7977749087	2.8529056901
	32770	1.9974865732	2.0205195647	2.7976342689	2.8527077398
	Order	-1.948574297	-1.984750629	-1.994403897	-1.954185324
$\mathcal{T}_h^2$	962	2.0030212894	2.0264963831	2.8278490203	2.8951798743
	3458	1.9979686225	2.0210485062	2.8001920010	2.8562199340
	13058	1.9975202761	2.0205554732	2.7978153285	2.8529529025
	50690	1.9974870528	2.0205203038	2.7976375682	2.8527115591
	Order	-1.958513219	-1.987176322	-1.951483684	-1.960796880
$\mathcal{T}_h^3$	1026	2.0037732572	2.0268631357	2.8359368161	2.9022010958
	4098	1.9978823607	2.0208843513	2.7999054850	2.8558652671
	16386	1.9975095482	2.0205398168	2.7977620896	2.8528923783
	65538	1.9974862245	2.0205192701	2.7976335086	2.8527066453
	Order	-1.999811187	-2.034365717	-2.030077806	-2.000763197
$\mathcal{T}_h^4$	1922	2.0040024344	2.0281345170	2.8394901486	2.9094960218
	6914	1.9980913357	2.0212701094	2.8019792724	2.8588028070
	26114	1.9975313826	2.0205757251	2.7979852855	2.8531956721
	101378	1.9974878458	2.0205217537	2.7976499337	2.8527289077
	Order	-1.922026073	-1.922266649	-1.864099554	-1.870542146

5.4.2. 3D stabilization-free VEM

For any polyhedron E, let $F \in \partial E$ be a boundary face of E. As usual, the 2D virtual element space $V_h(F)$ in (3.2) can be seen as the boundary space of a 3D discrete space denoted by

$$B_h(\partial E) := \big\{ v \in C^0(\partial E) \,:\, v|_F \in V_h(F),\, \forall\, F \in \partial E \big\}. \tag{5.5}$$

Mimicking 2D case (3.2), the local stabilization-free virtual element space on the 3D element E is defined by

$$V_h(E) = \Big\{ v_h \in H^1(E) \cap C^0(\partial E) \,:\, v_h|_{\partial E} \in B_h(\partial E), \Delta v_h \in \mathbb{P}_{1+l}(E), \\ \int_E (v_h - \Pi_{1,E}^{\nabla} v_h) p_{1+l} \mathrm{d}E = 0,\ \forall\, p_{1+l} \in \mathbb{P}_{1+l}(E) \Big\}, \tag{5.6}$$

where the projection $\Pi^{\nabla}_{1,E}$ is defined by extending (3.1) to the 3D case. The local degrees of freedom of the 3D space $V_h(E)$ are endowed with the values of v_h at all vertices of E, see [2]. The global 3D stabilization-free VEM space can be defined by the same way as (3.3). To avoid repetitive arguments, we only concern the discrete version of the case $n \equiv 1$ in this subsection, i.e. the same discrete formulation as (3.12). Noticing that, in the practical computation, the most involved procedure is to compute the polynomial projection $\mathbf{\Pi}^0_{l,E}$ in the stabilization-VEM scheme (3.12). Indeed, for any $v_h \in V_h(E)$ and $\boldsymbol{p}_l \in [\mathbb{P}_l(E)]^3$, it follows by the definition of $\mathbf{\Pi}^0_{l,E}$ and integrating by part that

$$\begin{aligned}\int_E \mathbf{\Pi}^0_{l,E}\nabla v_h \cdot \boldsymbol{p}_l \,\mathrm{d}E &= \int_E \nabla v_h \cdot \boldsymbol{p}_l \,\mathrm{d}E = \int_{\partial E} v_h \boldsymbol{p}_l \cdot \boldsymbol{\nu}_{\partial E} \,\mathrm{d}s - \int_E \mathrm{div}(\boldsymbol{p}_l) v_h \,\mathrm{d}E \\ &\overset{(5.6)}{=} \sum_{F\in\partial E} \int_F v_h \boldsymbol{p}_l \cdot \boldsymbol{\nu}_F \,\mathrm{d}F - \int_E \mathrm{div}(\boldsymbol{p}_l)\Pi^{\nabla}_{1,E} v_h \,\mathrm{d}E.\end{aligned}$$

Because the virtual function v_h restricted on the face F is not explicitly known, it follows from (5.5) and (3.2) that

$$\int_F v_h \boldsymbol{p}_l \cdot \boldsymbol{\nu}_F \,\mathrm{d}F = \int_F \big(\Pi^{\nabla}_{1,F} v_h\big)\boldsymbol{p}_l \cdot \boldsymbol{\nu}_F \,\mathrm{d}F.$$

Therefore, the vectorial polynomial projection $\mathbf{\Pi}^0_{l,E}$ is computable from the computation of the projection operators $\Pi^{\nabla}_{1,F}$ and $\Pi^{\nabla}_{1,E}$.

Here we take $\boldsymbol{A}(x,y) = (1/4)\boldsymbol{I}$ for $(x,y) \in \Omega_C = [0,1]^3$. This choice is in accordance with the reference eigenvalues in [42, Table 5] as follows:

$$k_1 = 5.2602, \quad k_2 = 5.9167, \quad k_3 = 5.9168, \quad k_2 = 5.9168,$$

obtained by the finite element method with 722772 degrees of freedom. We decompose the domain Ω_C with four sequence of polyhedral meshes: tetrahedral mesh $\mathcal{T}_h^5$ and other polyhedral meshes $\mathcal{T}_h^6, \mathcal{T}_h^7, \mathcal{T}_h^8$. These polyhedral meshes $\mathcal{T}_h^6, \mathcal{T}_h^7, \mathcal{T}_h^8$ are made by translating the 2D polygonal meshes $\mathcal{T}_h^1, \mathcal{T}_h^2, \mathcal{T}_h^3$ in Fig. 5.1 along the z-axis and connecting the corresponding vertices, see Fig. 5.7. In Table 5.8, we present numerical results of the transmission eigenvalues obtained by the stabilization-free VEM with $l = 3$. As usual, the mesh size h is expected to $h \approx N^{-1/3}$, then the optimal convergence order $\mathcal{O}(h^2)$ in Theorem 4.3 is equivalent to $\mathcal{O}(N^{-2/3})$ with respect to the degrees of freedom, that is, the numerical method achieves the optimal convergence behavior in the 3D case.

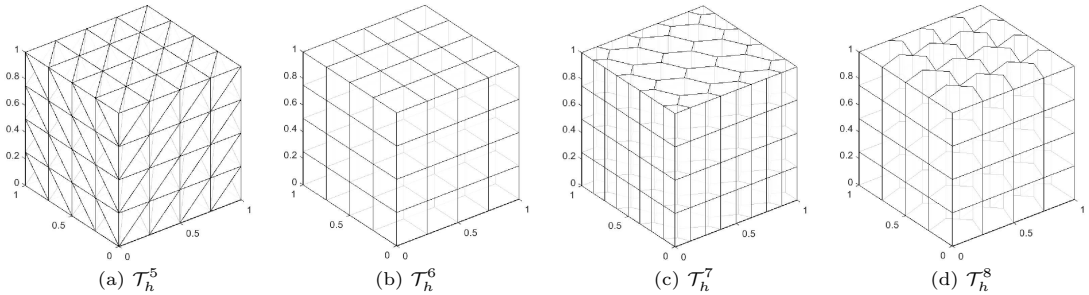

(a) $\mathcal{T}_h^5$ (b) $\mathcal{T}_h^6$ (c) $\mathcal{T}_h^7$ (d) $\mathcal{T}_h^8$

Fig. 5.7. Test 5.4.2: Sample meshes on Ω_C.

Table 5.8: Test 5.4.2: The first four real transmission eigenvalues on Ω_C ($n \equiv 1$ and $l = 3$).

Mesh	N	$k_{1,h}$	$k_{2,h}$	$k_{3,h}$	$k_{4,h}$
$\mathcal{T}_h^5$	154	8.6176159331	8.6777733358	8.6777733358	9.7740062760
	1074	5.9487898727	6.6677159763	6.6677159763	7.4153368120
	8290	5.4246822857	6.1004989772	6.1004989772	6.3233070838
	Order	-0.700626808	-0.688756592	-0.688756592	-0.638385599
$\mathcal{T}_h^6$	154	9.5422156025	11.759955603	11.759955603	11.759955603
	1074	7.1785056073	8.0255957317	8.0255957317	8.0255957317
	8290	5.5442496032	6.3640496442	6.3640496442	6.3640496442
	Order	-0.712480286	-0.758726632	-0.758726632	-0.758726632
$\mathcal{T}_h^7$	464	9.2916386985	10.565609438	11.171701324	11.296489109
	1865	6.7804151703	7.6749153647	7.8968095912	8.0545733597
	7534	5.7336925764	6.5546851576	6.6659818245	6.7085331325
	Order	-0.835482111	-0.726088618	-0.696103410	-0.711445752
$\mathcal{T}_h^8$	674	7.2567776885	9.9096834411	10.87929432	11.323238467
	2866	5.9084601224	7.1642257471	7.247437044	7.4466283873
	11858	5.4712285814	6.3389227419	6.383002813	6.4106253838
	Order	-0.790303488	-0.762900917	-0.738541720	-0.796240035

6. Conclusion

In this paper, we have proposed the stabilization-free VEM for the TEP on anisotropic media with both $n \neq 1$ and $n \equiv 1$. Our main theoretical result is that the present stabilization-free VEMs achieve the optimal convergence. Numerical examples showed the capability of the stabilization-free VEM

(1) the validity and the optimal convergence,
(2) the virtues applied to the TEP on anisotropic media,
(3) the extensions to more general cases, including high-order numerical algorithm and 3D model.

Some negative aspects of the current stabilization-free VEM should be noticed. The theoretical aspect of the stability analysis for the stabilization-free VEM of general order is missing, thus, the method still needs a guaranteed theoretical backbone. Meanwhile, the cost to build the local matrix for the stabilization-free VEM is very high, because it has to use polynomials of much higher-order with respect to the original one. The upcoming article shall balance and investigate both. Moreover, the stabilization-free a posteriori error analysis for the VEM of the TEP is under consideration.

Acknowledgements. We would like to acknowledge the referees for constructive comments and suggestions.

This work is supported by the National Natural Science Foundation of China (Grant Nos. 12301532, 12271523, 12071481, 12371198, 12371374), by the Defense Science Foundation of China (Grant Nos. 2021-JCJQ-JJ-0538, 2022-JCJQ-JJ-0879), by the National Key Research

and Development Program of China (Grant No. 2020YFA0709803), by the Science and Technology Innovation Program of Hunan Province (Grant Nos. 2022RC1192, 2021RC3082), by the Natural Science Foundation of Hunan (Grant No. 2021JJ20053), and by the National University of Defense Technology (Grant Nos. 2023-lxy-fhjj-002, 202401-YJRC-XX-001).

References

[1] S. Agmon, *Lectures on Elliptic Boundary Value Problems*, in: *Van Nostrand Mathematical Studies*, Vol. 2, Princeton, 1965.

[2] B. Ahmad, A. Alsaedi, F. Brezzi, L. Marini, and A. Russo, Equivalent projections for virtual element methods, *Comput. Math. Appl.*, **66** (2013), 376–391.

[3] J. An and J. Shen, A spectral-element method for transmission eigenvalue problems, *J. Sci. Comput.*, 57 (2013), 670–688.

[4] P. Antonietti, L. Beirão Da Veiga, and G. Manzini, *The Virtual Element Method and Its Applications*, in: *SEMA SIMAI Springer Series*, Vol. 31, Springer, 2022.

[5] P. Antonietti, S. Berrone, A. Borio, A. D'Auria, M. Verani, and S. Weisser, Anisotropic a posteriori error estimate for the virtual element method, *IMA J. Numer. Anal.*, **42** (2022), 1273-1312.

[6] I. Babuška and J. Osborn, Finite element Galerkin approximation of the eigenvalues and eigenfunctions of selfadjoint problems, *Math. Comp.*, **52** (1989), 275–297.

[7] I. Babuška and J. Osborn, Eigenvalue problems, in: *Handbook of Numerical Analysis*, Elsevier Science Publishers, Vol. 2, (1991), 641–787.

[8] L. Beirão Da Veiga, F. Brezzi, A. Cangiani, G. Manzini, L. Marini, and A. Russo, Basic principles of virtual element methods, *Math. Models Methods Appl. Sci.*, **23** (2013), 199–214.

[9] L. Beirão Da Veiga, F. Brezzi, F. Dassi, L. Marini, and A. Russo, A family of three-dimensional virtual elements with applications to magnetostatics, *SIAM J. Numer. Anal.*, **56** (2018), 2940–2962.

[10] L. Beirão Da Veiga, F. Brezzi, L. Marini, and A. Russo, The hitchhiker's guide to the virtual element method, *Math. Models Methods Appl. Sci.*, **24** (2014), 1541–1573.

[11] L. Beirão Da Veiga, F. Brezzi, L. Marini, and A. Russo, Virtual element methods for general second-order elliptic problems on polygonal meshes, *Math. Models Methods Appl. Sci.*, **26** (2016), 729–750.

[12] L. Beirão Da Veiga, C. Lovadina, and G. Vacca, Divergence free virtual elements for the Stokes problem on polygonal meshes, *ESAIM Math. Model. Numer. Anal.*, **51** (2017), 509–535.

[13] L. Beirão Da Veiga and L. Mascotto, Stability and interpolation properties of serendipity nodal virtual elements, *Appl. Math. Lett.*, **142** (2023), 108639.

[14] L. Beirão Da Veiga, D. Mora, G. Rivera, and R. Rodriguez, A virtual element method for the acoustic vibration problem, *Numer. Math.*, **136** (2017), 725–763.

[15] S. Berrone, A. Borio, and F. Marcon, Comparison of standard and stabilization free virtual elements on anisotropic elliptic problems, *Appl. Math. Lett.*, **129** (2022), 107971.

[16] S. Berrone, A. Borio, and F. Marcon, Lowest order stabilization free virtual element method for the 2D Poisson equation, *arXiv:2103.16896v4*, 2023.

[17] S. Berrone, A. Borio, F. Marcon, and G. Teora, A first-order stabilization-free Virtual Element Method, *Appl. Math. Lett.*, **142** (2023), 108641.

[18] D. Boffi, Finite element approximation of eigenvalue problems, *Acta Numer.*, **19** (2010), 1–120.

[19] D. Boffi, F. Brezzi, and F. Fortin, *Mixed Finite Element Methods and Applications*, in: *Springer Series in Computational Mathematics*, Vol. 44, Springer, 2013.

[20] D. Boffi, F. Gardini, and L. Gastaldi, Approximation of PDE eigenvalue problems involving parameter dependent matrices, *Calcolo*, **57** (2020), 41.

[21] S. Brenner and R. Scott, *The Mathematical Theory of Finite Element Methods*, Springer-Verlag, 2008.

[22] F. Cakoni, D. Colton, and H. Haddar, The computation of lower bounds for the norm of the index of refraction in an anisotropic media from far field data, *J. Integral Equations Appl.*, **21** (2009), 203–227.

[23] F. Cakoni, D. Colton, and H. Haddar, *Inverse Scattering Theory and Transmission Eigenvalues*, SIAM, 2016.

[24] F. Cakoni and H. Haddar, Transmission eigenvalues in inverse scattering theory, in: *Inverse Problems and Applications. Inside Out II, MSRI Publications*, **60** (2012), 527–578.

[25] S. Cao, L. Chen, and R. Guo, Immersed virtual element methods for electromagnetic interface problems in three dimensions, *Math. Models Methods Appl. Sci.*, **33** (2023), 455–503.

[26] A. Chen and N. Sukumar, Stabilization-free serendipity virtual element method for plane elasticity, *Comput. Methods Appl. Mech. Engrg.*, **404** (2023), 115784.

[27] A. Chen and N. Sukumar, Stabilization-free virtual element method for plane elasticity, *Comput. Math. Appl.*, **138** (2023), 88–105.

[28] C. Chen, X. Huang, and H. Wei, H^m-conforming virtual elements in arbitrary dimension, *SIAM J. Numer. Anal.*, **60** (2022), 3099–3123.

[29] L. Chesnel and J.P. Ciarlet, T-coercivity and continuous Galerkin methods: Application to transmission problems with sign changing coefficients, *Numer. Math.*, **124** (2013), 1–29.

[30] D. Colton and R. Kress, *Inverse Acoustic and Electromagnetic Scattering Theory*, in: *Applied Mathematical Sciences*, Vol. 93, Springer, 2019.

[31] D. Colton, P. Monk, and J. Sun, Analytical and computational methods for transmission eigenvalues, *Inverse Problems*, **26** (2010), 045011.

[32] J. Descloux, N. Nassif, and J. Rappaz, On spectral approximation. Part 1. The problem of convergence, *RAIRO Anal. Numér.*, **12** (1978), 97–112.

[33] D. Gallistl and V. Olkhovskiy, Computational lower bounds of the Maxwell eigenvalues, *SIAM J. Numer. Anal.*, **61** (2023), 539–561.

[34] F. Gardini and G. Vacca, Virtual element method for second-order elliptic eigenvalue problems, *IMA J. Numer. Anal.*, **38** (2017), 2026–2054.

[35] B. Gong, J. Sun, T. Turner, and C. Zheng, Finite element/holomorphic operator function method for the transmission eigenvalue problem, *Math. Comput.*, **91** (2022), 2517–2537.

[36] I. Harris, F. Cakoni, and J. Sun, Transmission eigenvalues and non-destructive testing of anisotropic magnetic materials with voids, *Inverse Problems*, **30** (2014), 035016.

[37] X. Ji and J. Sun, A multi-level method for transmission eigenvalues of anisotropic media, *J. Comput. Phys.*, **255** (2013), 422–435.

[38] A. Kleefeld and D. Colton, Interior transmission eigenvalues for anisotropic media, in: *Integral Methods in Science and Engineering*, Birkhäuser, Vol. 1, (2017), 139–147.

[39] A. Kleefeld and L. Pieronek, Computing interior transmission eigenvalues for homogeneous and anisotropic media, *Inverse Problems*, **34** (2018), 105007.

[40] F. Lepe, D. Mora, G. Rivera, and I. Velásquez, A virtual element method for the Steklov eigenvalue problem allowing small edges, *J. Sci. Comput.*, **88** (2021), 44.

[41] F. Lepe and G. Rivera, A virtual element approximation for the pseudostress formulation of the Stokes eigenvalue problem, *Comput. Methods Appl. Mech. Engrg.*, **379** (2021), 113753.

[42] Q. Liu, T. Li, and S. Zhang, A mixed element scheme for the Helmholtz transmission eigenvalue problem for anisotropic media, *Inverse Problems*, **39** (2023), 055005.

[43] J. Meng, Discontinuous Galerkin method for the interior transmission eigenvalue problem in inverse scattering theory, *J. Sci. Comput.*, **96** (2023), 66.

[44] J. Meng and L. Mei, Virtual element method for the Helmholtz transmission eigenvalue problem of anisotropic media, *Math. Models Methods Appl. Sci.*, **32** (2022), 1589–1631.

[45] J. Meng, G. Wang, and L. Mei, A lowest-order virtual element method for the Helmholtz transmission eigenvalue problem, *Calcolo*, **58** (2021), 2.

[46] J. Meng, G. Wang, and L. Mei, Mixed virtual element method for the Helmholtz transmission

eigenvalue problem on polytopal meshes, *IMA J. Numer. Anal.*, **43** (2023), 1685–1717.
[47] D. Mora, G. Rivera, and R. Rodríguez, A virtual element method for the Steklov eigenvalue problem, *Math. Models Methods Appl. Sci.*, **25** (2015), 1421–1445.
[48] D. Mora and I. Velásquez, A virtual element method for the transmission eigenvalue problem, *Math. Models Methods Appl. Sci.*, **28** (2018), 2803–2831.
[49] D. Mora and I. Velásquez, Virtual element for the buckling problem of Kirchhoff-Love plates, *Comput. Methods Appl. Mech. Engrg.*, **360** (2020), 112687.
[50] D. Mora and I. Velásquez, Virtual elements for the transmission eigenvalue problem on polytopal meshes, *SIAM J. Sci. Comput.*, **43** (2021), A2425–A2447.
[51] J. Sun, Iterative methods for transmission eigenvalues, *SIAM J. Numer. Anal.*, **49** (2011), 1860–1874.
[52] C. Talischi, G. Paulino, A. Pereira, and I. Menezes, Polymesher: A general-purpose mesh generator for polygonal elements written in Matlab, *Struct. Multidiscip. Optim.*, **45** (2012), 309–328.
[53] M.E. Taylor, *Partial Differential Equations*, Springer, 2023.
[54] G. Wang, J. Meng, Y. Wang, and L. Mei, A priori and a posteriori error estimates for a virtual element method for the non-self-adjoint Steklov eigenvalue problem, *IMA J. Numer. Anal.*, **42** (2022), 3675–3710.
[55] Y. Xi, X. Ji, and S. Zhang, A high accuracy nonconforming finite element scheme for Helmholtz transmission eigenvalue problem, *J. Sci. Comput.*, **83** (2020), 67.
[56] H. Xie and X. Wu, A multilevel correction method for interior transmission eigenvalue problem, *J. Sci. Comput.*, **72** (2017), 586–604.
[57] Y. Yang, H. Bi, H. Li, and J. Han, Mixed methods for the Helmholtz transmission eigenvalues, *SIAM J. Sci. Comput.*, **38** (2016), A1383–A1403.
[58] Y. Yang, J. Han, and H. Bi, H^2-conforming methods and two-grid discretizations for the elastic transmission eigenvalue problem, *Commun. Comput. Phys.*, **28** (2020), 1366–1388.